

## 1                    **Prevention and therapy of SARS-CoV-2 and the B.1.351 variant in mice**

2  
3 David R. Martinez<sup>1,7,\*</sup>, Alexandra Schaefer<sup>1,7</sup>, Sarah R. Leist<sup>1</sup>, Dapeng Li<sup>2</sup>, Kendra Gully<sup>1</sup>,  
4 Boyd Yount<sup>1</sup>, Joy Y. Feng<sup>3</sup>, Elaine Bunyan<sup>3</sup>, Danielle P. Porter<sup>3</sup>, Tomas Cihlar<sup>3</sup>, Stephanie A.  
5 Montgomery<sup>4</sup>, Barton F. Haynes<sup>2</sup>, Ralph S. Baric<sup>1</sup>, Michel C. Nussenzweig<sup>5,6</sup>, Timothy P.  
6 Sheahan<sup>1,\*</sup>.

7  
8 <sup>1</sup> Department of Epidemiology, READDI Initiative, University of North Carolina at Chapel Hill,  
9 Chapel Hill, NC, USA,

10  
11 <sup>2</sup> Duke Human Vaccine Institute, Duke University, Durham, NC, USA.

12  
13 <sup>3</sup> Gilead Sciences, Inc, Foster City, CA, USA

14  
15 <sup>4</sup> Department of Pathology and Laboratory Medicine, University of North Carolina School of  
16 Medicine, Chapel Hill, NC, USA,

17  
18 <sup>5</sup> The Rockefeller University, New York, NY, USA

19  
20 <sup>6</sup> The Howard Hughes Medical Institute, Chevy Chase, MD, USA

21  
22 <sup>7</sup> Equal contribution

23  
24 \* Correspondence: David R. Martinez, [david.rafael.martinez@gmail.com](mailto:david.rafael.martinez@gmail.com); Timothy P. Sheahan.  
25 [sheahan@email.unc.edu](mailto:sheahan@email.unc.edu)

26  
27  
28 **KEYWORDS:** SARS-CoV-2, B.1.351, variants, remdesivir, RDV, monoclonal antibodies,  
29 COVID-19, therapy.

### 30 31 **SUMMARY**

32                    Improving the standard of clinical care for individuals infected with SARS-CoV-2  
33 variants is a global health priority. Small molecule antivirals like remdesivir (RDV) and  
34 biologics such as human monoclonal antibodies (mAb) have demonstrated therapeutic efficacy  
35 against SARS-CoV-2, the causative agent of COVID-19. However, it is not known if  
36 combination RDV/mAb will improve outcomes over single agent therapies or whether antibody  
37 therapies will remain efficacious against variants. In kinetic studies in a mouse-adapted model of

38 ancestral SARS-CoV-2 pathogenesis, we show that a combination of two mAbs in clinical trials,  
39 C144 and C135, have potent antiviral effects against even when initiated 48 hours after infection.  
40 The same antibody combination was also effective in prevention and therapy against the B.1.351  
41 variant of concern (VOC). Combining RDV and antibodies provided a modest improvement in  
42 outcomes compared to single agents. These data support the continued use of RDV to treat  
43 SARS-CoV-2 infections and support the continued clinical development of the C144 and C135  
44 antibody combination to treat patients infected with SARS-CoV-2 variants.

45

## 46 INTRODUCTION

47 A novel human coronavirus, SARS-CoV-2, emerged in late 2019 in Wuhan, China (Zhou  
48 et al., 2020b; Zhu et al., 2020) as the causative agent of coronavirus disease 2019 (COVID-19).  
49 The spread of SARS-CoV-2 was explosive with ~140 million confirmed cases and >3 million  
50 deaths worldwide as of April 2021. Few therapies are available to treat COVID-19 disease in  
51 humans and the rapid evolution of SARS-CoV-2 variants threatens to diminish their efficacy.  
52 Remdesivir (RDV, Veklury) is the only U.S. Food and Drug Administration (FDA) approved  
53 direct-acting, small molecule antiviral to treat COVID-19. Prior to the emergence of SARS-CoV-  
54 2, RDV showed broad-spectrum activity against highly pathogenic human coronaviruses  
55 including SARS-CoV, MERS-CoV, their related enzootic viruses, and endemic common-cold  
56 causing coronaviruses (CoV) in various *in vitro* and *in vivo* preclinical models of CoV  
57 pathogenesis (Brown et al., 2019; de Wit et al., 2020; Sheahan et al., 2017; Sheahan et al., 2020).  
58 More recently, RDV was shown to exert potent antiviral activity against SARS-CoV-2 *in vitro*  
59 (Pruijssers et al., 2020) and therapeutic efficacy in a SARS-CoV-2 rhesus macaque model, which  
60 recapitulates mild to moderate respiratory symptoms (Williamson et al., 2020). In a double-blind,

61 randomized, placebo-controlled trial (ACTT-1), RDV was shown to shorten recovery time in  
62 hospitalized COVID-19 patients by 5 days on average as compared to those receiving placebo  
63 (Beigel et al., 2020). In contrast, in an open-label, non-placebo-controlled, and non-blinded  
64 clinical trial (WHO Solidarity trial) RDV was not shown to improve outcomes in hospitalized  
65 patients (Wang et al., 2020). Importantly, mutations in the viral RNA dependent RNA  
66 polymerase (RdRp) known to interfere with the antiviral activity of RDV are not found in the  
67 identifying amino acid signatures of SARS-CoV-2 VOCs (Martin et al., 2021). As combinations  
68 of RDV with immunomodulators (Baricitinib) have very recently been shown to improve  
69 COVID-19 outcomes over single-agent treatment (Kalil et al., 2020), it remains unknown  
70 whether RDV combinations with other antiviral drugs with complementary modalities will yield  
71 similarly promising results.

72         Several monoclonal antibodies (mAb) targeting the SARS-CoV-2 spike have been shown  
73 to potently neutralize SARS-CoV-2 *in vitro* (Dieterle et al., 2020; Jones et al., 2020; Li et al.,  
74 2021; Robbiani et al., 2020; Rogers et al., 2020; Yang et al., 2020; Zost et al., 2020a; Zost et al.,  
75 2020b). Monoclonal antibody (mAb) drugs targeting the SARS-CoV-2 spike have demonstrated  
76 therapeutic efficacy in multiple pre-clinical models of viral pathogenesis, and a select few have  
77 been authorized for emergency use by the FDA to treat COVID-19 (Ly-CoV016/LyCoV555, Eli  
78 Lilly; REGN10987/ REGN10933, Regeneron)(2020a; Barnes et al., 2020a; Barnes et al., 2020b;  
79 Jones et al., 2020; Schäfer et al., 2021). Most clinical candidate mAbs are RBD-specific and  
80 have varying modes of binding and epitope specificities (Barnes et al., 2020a). Lilly's LY-  
81 CoV555 can recognize the RBD in both the up and down conformations (Jones et al., 2020).  
82 REGN10987 binds to the RBD outside the ACE2 binding site whereas REGN10933 binds to the  
83 top of the RBD and competes with the ACE2 binding site (Hansen et al., 2020). Two recently

84 described highly potent SARS-CoV-2 neutralizing mAbs, C144 and C135, currently being  
85 evaluated in human trials at the Rockefeller University Hospital (ClinicalTrials.gov Identifier:  
86 NCT04700163) and licensed to Bristol Myers Squibb for development (Robbiani et al., 2020).  
87 C144 ( $IC_{50} = 2.55$  ng/mL) and C135 ( $IC_{50} = 2.98$  ng/mL), were isolated from convalescent  
88 human patients and target non-overlapping sites on the receptor binding domain (RBD) on the  
89 SARS-CoV-2 spike protein similar to the REGN mAb cocktail (Barnes et al., 2020a; Barnes et  
90 al., 2020b; Robbiani et al., 2020; Schäfer et al., 2021). As mAb prophylaxis can prevent COVID-  
91 19, preliminary results from human clinical trials evaluating the therapeutic efficacy of mAbs in  
92 COVID-19 outpatients have thus far been promising (Weinreich et al., 2020; Zhou et al., 2020b).

93 The emergence of SARS-CoV-2 variants that can partially or completely evade mAbs in  
94 advanced clinical development is a growing concern. For example, the SARS-CoV-2 South  
95 African B.1.351 variant can completely evade neutralization by mAb LY-CoV555 (Wang et al.,  
96 2021a; Wang et al., 2021b). Other mAbs in clinical development, including the AstraZeneca  
97 COV2-2196 mAb and the Bria BioSciences mAb Bria-198, have a reduction in neutralization  
98 potency by more than 6-fold due to the presence of the E484K mutation (Chen et al., 2021;  
99 Wang et al., 2021b). Moreover, the neutralization activity of the Regeneron mAb REGN 10933,  
100 is also dampened by the E484K mutation (Wang et al., 2021b). In contrast, the variants do not  
101 affect the neutralization potency of C135 (Wang et al., 2021b). Lastly, while the variants do not  
102 affect the C144 + C135 antibody combination *in vitro* (Wang et al., 2021c), it is not yet known if  
103 this mAb cocktail can protect against the SARS-CoV-2 variants *in vivo*.

104 We previously developed a mouse-adapted model of SARS-CoV-2 (SARS-CoV-2  
105 MA10) pathogenesis based on the ancestral pandemic strain (Leist et al., 2020). Following  
106 SARS-CoV-2 MA10 infection of standard laboratory mice, virus replicates primarily in ciliated

107 epithelial cells and type II pneumocytes with peak titers by 48 hours post infection (hpi)  
108 concurrent with body weight loss, loss of pulmonary function, the development of acute lung  
109 injury (ALI) and mortality, consistent with severe human COVID-19 pathogenesis (Leist et al.,  
110 2020). Here, we define the prophylactic and therapeutic efficacy of RDV and C144 + C135  
111 mAbs used singly and in combination in mice infected with SARS-CoV-2 MA10. We show that  
112 the prophylactic and therapeutic administration of RDV or mAb exert a robust antiviral effect  
113 and their ability to abrogate disease diminished as a function of initiation time. When combined,  
114 RDV/mAb therapy modestly improved outcomes compared to monotherapy suggesting that  
115 combination therapy may provide an additional therapeutic benefit over single agents in humans  
116 with COVID-19. Importantly, we demonstrate that C144 + C135 mAb combination protects  
117 from severe disease against SARS-CoV-2 South African B.1.351 variant challenge in an mouse  
118 model of age-related COVID-19 pathogenesis. These data support the continued use of RDV to  
119 treat SARS-CoV-2 infections and support the continued clinical development of the C144 and  
120 C135 antibody combination to treat patients infected with SARS-CoV-2 variants.

121

122

## 123 **RESULTS**

124

### 125 **Prophylactic and therapeutic RDV protect against COVID-19 disease in mice.**

126 First, we sought to determine the time at which RDV therapy would fail to improve outcomes in  
127 SARS-CoV-2 infected mice. Due to a serum esterase absent in humans but present in mice that  
128 reduces RDV stability (carboxyesterase 1c (*Ces1c*)), we performed all of our RDV efficacy  
129 studies in C57BL/6 mice lacking this gene (*Ces1c*<sup>(-/-)</sup>) (Sheahan et al., 2017). Although we had

130 previously explored the *in vivo* efficacy of RDV against SARS-CoV/SARS-CoV-2 chimeric  
131 viruses (Pruijssers et al., 2020), we had not yet evaluated RDV in mice infected with our recently  
132 described mouse adapted SARS-CoV-2 (SARS-CoV-2 MA10) (Leist et al., 2020). We initiated  
133 twice-daily treatment of mice with a human equivalent dose of RDV (25mg/kg) or vehicle -12  
134 hours prior to infection or 12 (early), 24 (mid-late), or 48 (late) hours post infection (hpi) with  $1$   
135  $\times 10^4$  particle forming units (PFU) of SARS-CoV-2 MA10. Body weight loss is a crude marker  
136 of emerging coronavirus disease in mice. Body weight loss observed in vehicle treated animals  
137 was prevented with prophylactic RDV (Figure 1A). When initiated after SARS-CoV-2 infection,  
138 only early therapeutic intervention (+12hr) was able to significantly diminish weight loss (Figure  
139 1A). While RDV therapy initiated at 24hr did not prevent weight loss, lung viral load was  
140 significantly diminished in this group similar to those receiving prophylaxis (-12hr) or early  
141 therapeutic intervention (+12hr) (Figure 1B). Similarly, lung discoloration, a gross pathologic  
142 feature characteristic of severe lung damage, was observed in the vehicle-treated animals but was  
143 diminished in all treatment groups except the 48hpi RDV group (Figure 1C). We then used a  
144 histologic tool developed by The American Thoracic Society (ATS) to quantitate the  
145 pathological features of ALI that we recently utilized to examine the pulmonary pathology of  
146 SARS-CoV-2 MA10 infected BALB/c mice (Leist et al., 2020; Matute-Bello et al., 2011). Per  
147 animal, three random diseased fields in lung tissue sections were blindly evaluated by a board-  
148 certified veterinary pathologist for alveolar septal thickening, protein exudate in the airspace,  
149 hyaline membrane formation, and neutrophils in the interstitium or airspaces. Scoring revealed  
150 that RDV prophylaxis and therapy initiated at both +12 and +24 hpi reduced ALI as compared to  
151 vehicle treated animals (Figure 1D and Figure S1). A complementary histological tool measuring  
152 the pathological hallmark of ALI, diffuse alveolar damage (DAD), revealed consistent data

153 (Figure 1E and Figure S1) with those in Figure 1D (Schmidt et al., 2018; Sheahan et al., 2020).  
154 Lastly, pulmonary function was measured daily in a subset of mice per group (N = 4) by whole-  
155 body plethysmography (WBP). As shown with the WBP metric enhanced pause (PenH), a metric  
156 for airway resistance or obstruction that was previously validated in animal models of CoV  
157 pathogenesis (Menachery et al., 2015; Sheahan et al., 2017), only prophylactic and early  
158 therapeutic administration of RDV (+12hpi) prevented the loss of pulmonary function observed  
159 in the other groups. Together, these data show that prophylactic and therapeutic RDV exerts a  
160 profound antiviral effect when administered up to 24hpi but the ability of RDV therapy to  
161 improve disease outcomes wanes with time of initiation.

162

163 **Prophylactic and therapeutic single mAb and mAb combinations reduce SARS-CoV-2**  
164 **pathogenesis.**

165 In COVID-19 patients, the time at which mAb therapy loses its protective effect remains  
166 unknown. To address this, we sought to determine the prophylactic and therapeutic efficacy of a  
167 cocktail of clinical candidate mAbs, C144 and C135, in the SARS-CoV-2 MA10 pathogenesis  
168 model noted above. We first established therapeutic efficacy profiles for single mAbs. We  
169 treated C57BL/6 mice with mAb C144, mAb C135 or control HIV mAb 12hr before or 12, 24, or  
170 48hr after infection with  $1 \times 10^4$  PFU of SARS-CoV-2 MA10 (Figure S3, S4, S5 and S6). Both  
171 mAbs significantly prevented (prophylactic) or reduced (+12hr, +24hr) SARS-CoV-2 MA10  
172 pathogenesis (body weight loss, lung discoloration, ALI scores, etc.) with C135 exerting more  
173 robust protection over C144 with measurable improvements in weight loss and gross pathology  
174 even when initiated 48 hpi (Figure S3, S4, and S5). Unlike C135 mAb, C144 mAb did not  
175 completely prevent virus replication in the lung when administered at 24hpi suggesting

176 incomplete viral breakthrough (Figure S4) likely driven by mouse adapting Q493K spike  
177 mutation which resides in a region critical for C144 binding (Barnes et al., 2020a; Barnes et al.,  
178 2020b; Gaebler et al., 2021; Leist et al., 2020). Neither antibody when administered 48hpi could  
179 prevent weight loss, lung discoloration or ALI yet viral lung titers were significantly reduced  
180 (Figure S6). Together, these data demonstrate that clinical candidate mAb C135 and C144 can  
181 both prevent and significantly diminish disease in an ongoing SARS-CoV-2 infection in mice.

182         Next, we evaluated the prophylactic and therapeutic efficacy of combination C144 +  
183 C135 to determine if the single agent therapeutic efficacy could be improved with mAb  
184 combinations. Similar to the studies with single agent mAb, we treated C57BL/6 mice with mAb  
185 combination C144 + C135 12hr prior to or 12, 24, or 48hr after infection with  $1 \times 10^4$  PFU of  
186 SARS-CoV-2 MA10. Unlike the uniform and consistent body weight loss observed in SARS-  
187 CoV-2 MA10 infected mice treated with negative control HIV mAb, prophylactic, early (+12hr)  
188 and mid-late (+24hr) therapeutic administration of C144 + C135 mAbs protected against  
189 bodyweight loss (Figure 2A). Initiation of therapy 48hpi afforded limited protection from body  
190 weight loss (Figure 2A). Remarkably, the levels of infectious virus in the lung were significantly  
191 reduced below the limit of detection (50 particle forming units, PFU) in all C144 + C135 mAb  
192 groups by day 5 post infection (dpi) unlike control mAb treated animals (mean lung titer =  $1 \times 10^4$   
193 PFU/lobe). Mirroring the trend observed in body weight loss, gross lung pathology as measured  
194 by observation of lung discoloration was eliminated with prophylactic C144 + C135 mAb,  
195 significantly diminished with early (+12hr) and mid-late (+24hr) dosing of C144 + C135 mAb  
196 and even moderately reduced with late (+48hr) therapy. We then quantitated the histologic  
197 features of ALI using the same tools employed in Figure 1 which demonstrated that prophylactic  
198 and therapy initiated up to 24hpi significantly reduced ALI observed in negative control mAb



199 treated animals (Figure 2D). When applying the DAD scoring tool to the same tissue sections,  
200 we saw a similar trend yet only prophylactic and early therapeutic (+12hr) C144 + C135  
201 significantly reduced scores (Figure 2E). In agreement with the histological assessment, loss of  
202 pulmonary function observed in negative control mAb treated animals could be prevented with  
203 prophylactic and early therapeutic (+12hpi) C144 + C135 (Figure 2F).  
204 Interestingly, combination mAb therapy initiated at 24hpi also provided a benefit in pulmonary  
205 function (Figure 2F). Thus, mAb therapy can exert a profound antiviral effect even when  
206 administered at later times post infection.

207

### 208 **Combination RDV/mAb cocktail demonstrates a small improvement vs mAb therapy alone** 209 **at 36hpi**

210 We sought to determine if combination RDV/C144+C135 mAb would further curtail  
211 viral pathogenesis over that provided by single agents. We designed a study where we initiated  
212 single agent or combination therapy 24hr after SARS-CoV-2 MA10 infection, treated mice up to  
213 7dpi and followed mice until 12dpi to determine if therapy accelerated recovery. Among groups  
214 receiving single agents or combination therapies, significant differences in body weight were not  
215 consistently noted (Figure S7A) but all therapeutic treatment groups provided complete  
216 protection from mortality observed with vehicle treatment (Figure S7B). Upon completion of the  
217 study on 12dpi, differences in gross pathology were not noted among treatment groups (Figure  
218 S7C). We performed pulmonary function by WBP on select groups (i.e. vehicle/control mAb and  
219 RDV/mAb combination) for the first 5 days of infection and observed a rapid improvement in  
220 pulmonary function with combination therapy which returned to baseline by 3dpi (Figure S7D).

221 To determine if a further delay treatment initiation time closer to peak of virus replication  
222 in the lung would reveal an improved benefit of combination therapy, we performed a  
223 therapeutic efficacy study initiating treatment at 36hpi. Rather than focus on the potential effects  
224 on recovery, the goal of this study was to determine if combination therapy had a differential  
225 effect on lung pathology and virus replication during the acute phase of disease. We initiated  
226 treatment 36hr after infection with  $1 \times 10^4$  PFU SARS-CoV-2 MA10 in C57BL/6 (*Ces1c*<sup>-/-</sup>)  
227 mice with the vehicle, single agent, and combination groups as described in the previous  
228 combination experiment. We observed a small but measurable improvement in body weight loss  
229 with RDV/mAb treatment (Figure 3A). Similarly, by 3dpi, only the RDV/control mAb and  
230 RDV/mAb-treated groups had lower lung viral titers compared to the vehicle/control mAb-  
231 treated group (Figure 3B). By 5dpi, vehicle treated animals had mean lung titers nearing  $1 \times 10^5$   
232 PFU, yet all treatment groups had significantly reduced lung titers at or near the limit of  
233 detection (Figure 3C). When examining gross lung pathology 5dpi, all therapies provided  
234 significant protection from lung discoloration observed with vehicle treatment, but RDV/mAb  
235 combination therapy group had the overall lowest score and was significantly improved over  
236 single agent vehicle/mAb (Figure 3D). We then quantitated the histological manifestations of  
237 ALI using the two complementary scoring tools employed above. With both ATS and DAD  
238 scoring systems, ALI was readily apparent in vehicle treated animals (Figure 3E and 3F).  
239 Although mirroring the trend observed in the gross pathological observations where combination  
240 therapy afforded protection over single agent therapy, significant differences were not observed  
241 among groups receiving antiviral therapies and all reduced ALI on 5dpi (Figure 3E and 3F).  
242 Lastly, we examined the effect of combination therapy on pulmonary function (Figure 3G).  
243 Combination RDV/mAb initiated at 36hpi reduced the loss of pulmonary function observed with

244 vehicle treatment on 3-5dpi (Figure 3G). Altogether, our findings suggest that combination  
245 therapy with RDV and potent neutralizing mAbs provides a small but measurable benefit over  
246 single agents in some but not all metrics of SARS-CoV-2 pathogenesis in this model.

247

248 **C144+C135 mAb prophylaxis and therapy improve outcomes in South African B.1.351**  
249 **variant of concern infected mice**

250 The emergence of neutralization-resistant SARS-CoV-2 variants is a growing threat.  
251 B.1.351, which initially emerged in South Africa, is a VOC that can infect mice without  
252 adaptation (Montagutelli et al., 2021). B.1.351 has characteristic RBD mutations at residues  
253 K417, E484, and N517 which result in resistance to many of the class 1 and 2 antibodies that  
254 dominate the initial RBD-directed neutralizing response (Barnes et al., 2020a; Chen et al., 2021;  
255 Planas et al., 2021; Wang et al., 2021c). For example, B.1.351 is completely resistant to Eli  
256 Lilly's Ly-CoV555 mAb (Wang et al., 2021a), underlining the importance of monitoring the *in*  
257 *vivo* efficacy of monoclonal antibody therapies that are in advanced clinical testing against  
258 SARS-CoV-2 VOCs. To examine the *in vivo* efficacy of the C144 + C135 mAb combination  
259 against recombinant mouse adapted SARS-CoV-2 bearing the B.1.351 spike, we treated aged  
260 BALB/c mice with mAb 12hr before or after infection with  $1 \times 10^4$  PFU. Weight loss observed  
261 with control antibody treatment was prevented with C144 + C135 prophylaxis and lung viral  
262 loads were reduced below the limit of detection on both 3 and 5dpi (Figure 4A-C). Similarly,  
263 mAb combination therapy accelerated recovery and diminished virus replication below the limit  
264 of detection by 5dpi (Figure 4A and 4C). To complement the infectious virus data, we then  
265 quantitated viral subgenomic RNAs in mouse lung tissues in each group. Unlike the quantitation  
266 of SARS-CoV-2 genomic RNA, which has the potential to measure RNA from infectious

267 particles, defective particles, mAb bound particles and various replicative forms of viral RNA,  
268 these subgenomic RNA qRT-PCR assays are specific for envelope (E) and nucleocapsid (N)  
269 viral transcripts which are only made in actively replicating cells. Prophylactic and therapeutic  
270 administration of C144 + C135 significantly reduced lung viral E sgRNA (Figure 4D and 4E)  
271 and N sgRNA (Figure 4F and 4G) compared to the control mAb treated animals indicating that  
272 mAb therapy successfully reduced levels of replication of SARS-CoV-2 bearing the B.1.351  
273 spike *in vivo*. Finally, gross pathology caused by mouse adapted SARS-CoV-2 bearing the  
274 B.1.351 spike was significantly reduced in aged mice with both prophylactic and therapeutic  
275 administration of the C144 + C135 combination (Figure 4H and 4I). Collectively, these data  
276 demonstrate that both prophylaxis and therapy with combination C144 + C135 mAb can potently  
277 reduce virus replication and improve disease outcomes *in vivo* following infection with variant  
278 B.1.351.

279

## 280 **DISCUSSION**

281 Therapies effective against the current and future SARS-CoV-2 VOCs are desperately  
282 needed to treat those yet to be vaccinated or those experiencing breakthrough infection. RDV is a  
283 broad-spectrum antiviral drug and has potent antiviral activity against multiple emerging,  
284 endemic and enzootic CoVs including: SARS-CoV, SARS-CoV-2, MERS-CoV, bat-CoV WIV-  
285 1, bat-CoV RsSHC014, bat-CoV HKU5, bat-CoV HKU-3-1, HCoV-229, HCoV-NL63, HCoV-  
286 OC43, porcine deltacoronavirus (PDCoV) (Agostini et al., 2018; Brown et al., 2019; de Wit et  
287 al., 2020; Sheahan et al., 2017). In addition to the *in vitro* activity of RDV against SARS-CoV-2  
288 (Pruijssers et al., 2020), RDV can exert an antiviral effect and diminish SARS-CoV-2 disease in  
289 rhesus macaques which develop mild respiratory disease (Williamson et al., 2020). Similarly, the

290 prophylactic efficacy of mAb C144 and C135 have previously been evaluated in replication  
291 models of mouse adapted SARS-CoV-2 based on the ancestral pandemic strain (Schäfer et al.,  
292 2021), but their prevention and therapy has not yet been evaluated in the context of the emerging  
293 variants that can evade vaccine-elicited antibodies and existing mAb therapies.

294 Human clinical data for direct antivirals like mAb and small molecule antivirals like  
295 RDV provides clear evidence that their success at improving outcomes is directly related to the  
296 time after the onset of symptoms that therapy is initiated. Outpatient studies evaluating mAb  
297 drugs in humans with mild to moderate COVID-19 demonstrated notable reductions in virus  
298 shedding and symptoms, which enabled the FDA emergency use authorization (EUA) of both Eli  
299 Lilly's and Regeneron's antibody cocktails (Gottlieb et al., 2021; Weinreich et al., 2020).  
300 However, hospitalized patients with advanced COVID-19 disease treated with these mAb drugs  
301 did not have measurably improved outcomes compared to standard of care (2020b). While RDV  
302 has been shown to accelerate recovery of COVID-19 hospitalized patients (Beigel et al., 2020),  
303 insight in to whether RDV will further improve outcomes in patients earlier in the course of  
304 COVID-19 remains unknown. Thus, the optimal window after the onset of symptoms within  
305 which to treat with antivirals such as RDV or potent mAbs fail remains unknown.

306 In this manuscript, we aimed to define the time after SARS-CoV-2 infection in mice  
307 where RDV or mAb therapy fail to exert an antiviral effect and/or fail to improve disease  
308 outcomes. Like mouse-adapted models of SARS-CoV and MERS-CoV, the replication kinetics  
309 of mouse-adapted SARS-CoV-2 MA10 in mice is compressed with peak replication in the lung  
310 48hpi (Leist et al., 2020). In contrast, the replication kinetics of SARS-CoV-2 in the airways of  
311 humans is more variable with reports estimating peak replication within the first week after the  
312 onset of symptoms (Liu et al., 2020; Zheng et al., 2020). Moreover, human patients can shed

313 viral RNA in the mucosa of the upper respiratory tract as long as 24 days post infection (Zhou et  
314 al., 2020a), underlining that sustained viral shedding and symptoms can last considerably longer  
315 in humans than mice. Thus, the window within which to intervene with antiviral therapy prior to  
316 the peak of virus replication in humans is dramatically different than in mice (~2 days). While  
317 our mouse model faithfully recapitulates many aspects of human COVID-19 disease (e.g. high  
318 titer replication in the upper and lower airway, loss of pulmonary function, acute lung injury, age  
319 related exacerbation of disease, etc.), it is not possible to very finely correlate the compressed  
320 kinetics of disease in mouse and those in humans but there are a few notable takeaways from the  
321 modeling presented herein. Given early therapeutic treatment at +12 and +24hpi in our model  
322 provided the most benefit, it is likely the benefit of antibody and small molecule antivirals like  
323 RDV will be maximized if given prior to peak viral replication and/or early in the disease course  
324 before patients are hospitalized. In addition, we show a small improvement with combination  
325 mAb/RDV over single agent therapy which suggests that combinations of antiviral drugs of  
326 disparate modalities may offer an additional benefit in COVID-19 patients over single agents,  
327 something that should be rigorously evaluated in humans. Although our studies clearly support  
328 the use/evaluation of RDV and mAb as treatments for COVID-19, both are administered  
329 intravenously limiting their broad distribution to COVID-19 outpatients. Potential strategies to  
330 allow the wider dissemination of these treatments may include chemical alteration of RDV to  
331 facilitate oral bioavailability and/or less complicated subcutaneous or intramuscular injections of  
332 mAbs. The effect of mAb injection route (i.e. subcutaneous vs. intravenous) on pharmacokinetics  
333 and safety is currently being evaluated for C144 and C135 in Phase I clinical studies  
334 (ClinicalTrials.gov Identifier: NCT04700163).

335           Given the growing emergence of SARS-CoV-2 variants, we examined the prophylactic  
336 and therapeutic efficacy of the C144 + C135 combination against the South African B.1.351  
337 variant spike in a robust age-related mouse model of SARS-CoV-2 pathogenesis. Importantly,  
338 the C144 + C135 cocktail demonstrated prophylactic and therapeutic efficacy against the B.1.351  
339 VOC, which is encouraging given that this variant has demonstrated full escape from other  
340 mAbs approved for emergency use in humans, such as the LY-CoV555. In addition, the  
341 neutralizing potency of the AstraZeneca and Bii Biosciences mAbs in clinical trials are clearly  
342 dampened by mutations present in the variants such as the B.1.351 (Wang et al., 2021b). The  
343 target of the antiviral activity of RDV is the viral RdRp. Importantly, hallmark mutations of  
344 current SARS-CoV-2 VOCs are not found in regions of the RdRp known to affect the antiviral  
345 potency of RDV, thus antiviral resistance to RDV is not currently anticipated with current VOCs  
346 (Martin et al., 2021). In context of emerging variants in the future, it will be critical to continue  
347 to evaluate the prevention and therapy of currently approved small molecule and mAb antivirals  
348 and those in clinical development against newly emerging variants of interest. Our results reveal  
349 that prophylaxis and therapy with the C144 + C135 mAb combination is robustly antiviral  
350 against the B.1.351 VOC spike *in vivo* and can diminish the development of disease during an  
351 ongoing SARS-CoV-2 infection in mice. These data support the further evaluation of this mAb  
352 cocktail as therapy in human patients infected with the B1.351 variant.

353

## 354 **STAR METHODS**

### 355 **Lead Contact**

356 Further information and requests for resources and reagents should be directed to and will be  
357 fulfilled by the Lead Contact, Timothy P. Sheahan ([sheahan@email.unc.edu](mailto:sheahan@email.unc.edu))

358 **Materials Availability**

359 Not applicable.

360 **Data and Code availability.**

361 Not applicable.

362

363 **EXPERIMENTAL MODEL AND SUBJECT DETAILS**

364

365 **Animals and virus infections**

366 Twenty-week-old male and female *Ces1c*<sup>(-/-)</sup> on a B6 background (C57BL/6J: Jackson  
367 Laboratory # 014096) were purchased from Jackson Laboratory. Eleven-month-old female  
368 BALB/c mice were purchased from Envigo (#047). A mouse-adapted SARS-CoV-2 virus  
369 (MA10) was used in all experiments and this virus was previously described (Leist et al., 2020).  
370 Briefly, mutations predictive of increased affinity to mouse ACE2 were introduced into a SARS-  
371 CoV-2 virus plasmid system and the virus was recovered by reverse genetics (Dinnon et al.,  
372 2020). This modified virus was then serially passaged in aged BALBc mice (Envigo #047) for  
373 ten passages which we refer to as the mouse-adapted passage 10 (MA10) SARS-CoV-2 (Leist et  
374 al., 2020). A mouse-adapted (MA10) backbone expressing the SARS-CoV-2 B.1.351 spike was  
375 generated for this study. All mice were anesthetized and infected with SARS-CoV-2 MA10 or  
376 B.1.351 spike/MA10 intranasally with  $1 \times 10^4$  PFU/ml. Mice were weighed daily and were  
377 monitored for signs of SARS-CoV-2 clinical disease in all experiments.

378

379 **Animal care**



380 The study was carried out in accordance with the recommendations for care and use of  
381 animals by the Office of Laboratory Animal Welfare (OLAW), National Institutes of Health and  
382 the Institutional Animal Care and Use Committee (IACUC) protocol number: 20-059 at  
383 University of North Carolina (UNC permit no. A-3410-01). Virus inoculations were performed  
384 under anesthesia and all efforts were made to minimize animal suffering. Animals were housed  
385 in groups and fed standard chow diets.

386

## 387 **METHOD DETAILS**

388

### 389 **Study design and treatment groups**

390 For the RDV experiment, a total of N=40, ~20-week-old male and female mice were  
391 divided into four groups each with N=10 mice with equal numbers of females and males in each  
392 group. RDV was administered subcutaneously twice per day (BID) at 25 mg/kg. Groups of N=10  
393 mice (N=5 males and N=5 females) were used in either the prophylaxis -12 hours before  
394 infection group, the early therapeutic 12 hours post infection group, the mid-late therapeutic 24  
395 hours post infection group, and the late therapeutic 48 hours post infection group.

396 For the initial monoclonal antibody experiment, mice were infected as described above  
397 and weighed daily and were monitored for signs of SARS-CoV-2 clinical disease. A total  
398 amount of 200 µg of C144 + C135, 200 µg of C144, 200 µg of C135, and 200 µg of HIV mAbs  
399 3BC117 + 10-1074 was administered intraperitoneally once by injection for each intervention  
400 group. Groups of N=20 female mice (N=5 mice treated with C144 + C135, N=5 mice treated  
401 with C144, N=5 mice treated with C135, and N=5 mice treated with 3BNC117 + 10-1074) were  
402 administered antibody 12 hours before infection, N=20 female mice (N=5 mice treated with

403 C144 + C135, N=5 mice treated with C144, N=5 mice treated with C135, and N=5 mice treated  
404 with 3BNC117 + 10-1074) were administered antibody 12hpi (early therapeutic group), N=20  
405 female mice (N=5 mice treated with C144 + C135, N=5 mice treated with C144, N=5 mice  
406 treated with C135, and N=5 mice treated with 3BNC117 + 10-1074) were administered antibody  
407 24hpi (mid-late therapeutic group), and N=20 female mice (N=5 mice treated with C144 + C135,  
408 N=5 mice treated with C144, N=5 mice treated with C135, and N=5 mice treated with 3BNC117  
409 + 10-1074) were administered antibody 48hpi (late therapeutic group).

410 For the 24hpi drug and mAb combination intervention experiment, a total of N=40, ~20-  
411 week-old male and female mice were divided into four groups each with N=10 mice with equal  
412 numbers of females and males in each group. At 24hpi, RDV treatment was initiated by  
413 subcutaneous injection twice per day (BID) at 25 mg/kg, and a total amount of 200 µg of C144 +  
414 C135 was administered intraperitoneally once by injection. N=10 mice (N=5 males and N=5  
415 females) were used in the vehicle + HIV mAb group. N=10 mice (N=5 males and N=5 females)  
416 were used in the vehicle + C144 + C135 mAb group. N=10 mice (N=5 males and N=5 females)  
417 were used in the RDV + HIV mAb group. N=10 mice (N=5 males and N=5 females) were used  
418 in the RDV + C144 + C135 mAb group.

419 For the 36hpi drug + mAb combination intervention experiment, a total of N=64, ~20-  
420 week-old male and female mice were divided into four groups each with N=16 mice with an  
421 equal number of females and males in each group. At 36hpi, RDV treatment was initiated by  
422 subcutaneous injection twice per day (BID) at 25 mg/kg, and a total of 200 µg of each  
423 monoclonal antibody treatment was administered intraperitoneally once by injection. N=32 mice  
424 were harvested at d3pi to evaluate early lung viral replication titers, and remaining mice were  
425 harvested at d5pi. N=16 mice (N=8 males and N=8 females) were used in the vehicle + HIV

426 mAb group. N=16 mice (N=8 males and N=8 females) were used in the vehicle + C144 + C135  
427 mAb group. N=16 mice (N=8 males and N=8 females) were used in the RDV + HIV mAb group.  
428 N=16 mice (N=8 males and N=8 females) were used in the RDV + C144 + C135 mAb group.

429

### 430 **Lung pathology scoring**

431 Acute lung injury was quantified via two separate lung pathology scoring scales: Matute-  
432 Bello and Diffuse Alveolar Damage (DAD) scoring systems. Analyses and scoring were  
433 performed by a Board Certified Veterinary Pathologist who was blinded to the treatment groups  
434 as described previously (Sheahan et al., 2020). Lung pathology slides were read and scored at  
435 600X total magnification.

436 The lung injury scoring system used is from the American Thoracic Society (Matute-  
437 Bello) in order to help quantitate histological features of ALI observed in mouse models to relate  
438 this injury to human settings. In a blinded manner, three random fields of lung tissue were  
439 chosen and scored for the following: (A) neutrophils in the alveolar space (none = 0, 1–5 cells =  
440 1, > 5 cells = 2), (B) neutrophils in the interstitial septae (none = 0, 1–5 cells = 1, > 5 cells = 2),  
441 (C) hyaline membranes (none = 0, one membrane = 1, > 1 membrane = 2), (D) Proteinaceous  
442 debris in air spaces (none = 0, one instance = 1, > 1 instance = 2), (E) alveolar septal thickening  
443 (< 2x mock thickness = 0, 2–4x mock thickness = 1, > 4x mock thickness = 2). To obtain a lung  
444 injury score per field, A–E scores were put into the following formula  $\text{score} = [(20 \times A) + (14 \times$   
445  $B) + (7 \times C) + (7 \times D) + (2 \times E)]/100$ . This formula contains multipliers that assign varying  
446 levels of importance for each phenotype of the disease state. The scores for the three fields per  
447 mouse were averaged to obtain a final score ranging from 0 to and including 1.

448 The second histology scoring scale to quantify acute lung injury was adopted from a lung  
449 pathology scoring system from lung RSV infection in mice (Schmidt et al., 2018). This lung  
450 histology scoring scale measures diffuse alveolar damage (DAD). Similar to the implementation  
451 of the ATS histology scoring scale, three random fields of lung tissue were scored for the  
452 following in a blinded manner: 1= absence of cellular sloughing and necrosis, 2=Uncommon  
453 solitary cell sloughing and necrosis (1–2 foci/field), 3=multifocal (3+foci) cellular sloughing and  
454 necrosis with uncommon septal wall hyalinization, or 4=multifocal (>75% of field) cellular  
455 sloughing and necrosis with common and/or prominent hyaline membranes. The scores for the  
456 three fields per mouse were averaged to get a final DAD score per mouse. The microscope  
457 images were generated using an Olympus Bx43 light microscope and CellSense Entry v3.1  
458 software.

459

#### 460 **Remdesivir (RDV)**

461 RDV was synthesized at Gilead Inc., and its chemical composition and purity were  
462 analyzed by nuclear magnetic resonance, high resolution mass spectrometry, and high-  
463 performance liquid chromatography. RDV was solubilized in 12% sulfobutylether- $\beta$ -  
464 cyclodextrin in water (with HCl/NaOH) at pH 5 for *in vivo* studies in mice. RDV was made  
465 available to UNC Chapel Hill under an existing material transfer agreement with Gilead Sciences  
466 Inc.

467

#### 468 **RNA extraction and subgenomic RNA assay**

469 Lung lobes were harvested and homogenized in 1ml of TRIzol reagent. RNA was  
470 extracted with phenol/chloroform/isoamyl alcohol solution (25:24:1), precipitated with isopropyl

471 alcohol, washed with 75% ethanol, and resuspended in RNAase-free water. SARS-CoV-2 E gene  
472 and N gene subgenomic mRNA (sgRNA) was measured by a one-step RT-qPCR adapted from  
473 previously described methods (Li et al., 2021). RNA extracted from animal samples  
474 or RNA standards were then measured using TaqMan Fast Virus 1-Step Master Mix  
475 (ThermoFisher, catalog # 4444432) and custom primers/probes targeting the E gene sgRNA  
476 (forward primer: 5' CGATCTCTTGTAGATCTGTTCTCE 3'; reverse primer: 5'  
477 ATATTGCAGCAGT ACGCACACA 3'; probe: 5' FAM  
478 ACACTAGCCATCCTTACTGCGCTTCG-BHQ1 3') or the N gene sgRNA (forward primer: 5'  
479 CGATCTCTTGTAGATCTGTTCTC 3'; reverse primer: 5' GGTGAA CCAAGACGCAGTAT  
480 3'; probe: 5' FAM-TAACCAGAATGGAGAACGCAGTG GG-BHQ1 3'). RT-QPCR reactions  
481 were carried out on a CFX Opus 384 machine (Bio-Rad) using a program below: reverse  
482 transcription at 50°C for 5 minutes, initial denaturation at 95°C for 20 seconds, then 40 cycles of  
483 denaturation-annealing-extension at 95°C for 15 seconds and 60°C for 30 seconds. Standard  
484 curves were used to calculate E or N sgRNA in copies per ml; the limit of detections (LOD) for  
485 both E and N sgRNA assays were 150 copies per lung lobe.

486  
487

## 488 **Biocontainment and biosafety**

489 Studies were approved by the UNC Institutional Biosafety Committee approved by  
490 animal and experimental protocols in the Baric laboratory. All work described here was  
491 performed with approved standard operating procedures for SARS-CoV-2 in a biosafety level 3  
492 (BSL-3) facility conforming to requirements recommended in the Microbiological and  
493 Biomedical Laboratories, by the U.S. Department of Health and Human Service, the U.S. Public

494 Health Service, and the U.S. Center for Disease Control and Prevention (CDC), and the National  
495 Institutes of Health (NIH).

496

#### 497 **Statistics**

498 All statistical analyses were performed using GraphPad Prism 9. Statistical tests used in  
499 each figure are denoted in the corresponding figure legend. A Sidak's multiple comparisons test  
500 was used following 2-way ANOVAs and this is also denoted in the figure legends.

501

#### 502 **Acknowledgements**

503 David R. Martinez is funded by a Burroughs Wellcome Fund Postdoctoral Enrichment  
504 Program Award, a Hanna H. Gray Fellowship from the Howard Hughes Medical Institute, and  
505 was supported by an NIH NIAID T32 AI007151 and an NIH F32 AI152296. This work was  
506 supported by NIAID R01 AI132178 awarded to Timothy P. Sheahan and Ralph S. Baric, and an  
507 NIH animal models contract (HHSN272201700036I) to R.S.B. This project was also supported  
508 by the North Carolina Policy Collaboratory at the University of North Carolina at Chapel Hill  
509 with funding from the North Carolina Coronavirus Relief Fund established and appropriated by  
510 the North Carolina General Assembly. Michel C. Nussenzweig is an investigator of the Howard  
511 Hughes Medical Institute. Animal histopathology services were performed by the Animal  
512 Histopathology & Laboratory Medicine Core at the University of North Carolina, which is  
513 supported in part by an NCI Center Core Support Grant (5P30CA016086-41) to the UNC  
514 Lineberger Comprehensive Cancer Center.

515

#### 516 **Author contributions**

517           Conceived the study: D.R.M, A.S., R.S.B, M.C.N., and T.P.S. Designed experiments:  
518 D.R.M, A.S., J.Y.F., E.B., D.P.P., T.C., R.S.B, M.C.N., and T.P.S. Performed laboratory  
519 experiments: D.R.M, A.S., S.R. L., D.L., K.G., T.P.S.; Provided critical reagents: J.Y.F., E.B.,  
520 D.P.P., T.C.; Wrote the first draft of the paper: D.R.M and T.P.S. Edited the manuscript: D.R.M,  
521 A.S., S.R. L., K.G., J.Y.F., E.B., D.P.P., T.C., S.A.M., B.F.H., R.S.B, M.C.N., and T.P.S. All  
522 authors reviewed and approved the manuscript.

523

524 **Conflict of interest**

525

526 J.Y.F., E.B., D.P.P., T.C. are employed by Gilead Sciences Inc.

527

528

529

530

531

532

533

534

535

536

537

538

539

## 540 REFERENCES

- 541 (2020a). An EUA for Bamlanivimab—A Monoclonal Antibody for COVID-19. *JAMA*.  
542 (2020b). A Neutralizing Monoclonal Antibody for Hospitalized Patients with Covid-19. *New*  
543 *England Journal of Medicine*.  
544 Agostini, M.L., Andres, E.L., Sims, A.C., Graham, R.L., Sheahan, T.P., Lu, X., Smith, E.C.,  
545 Case, J.B., Feng, J.Y., Jordan, R., *et al.* (2018). Coronavirus Susceptibility to the Antiviral  
546 Remdesivir (GS-5734) Is Mediated by the Viral Polymerase and the Proofreading  
547 Exoribonuclease. *mBio* 9.  
548 Barnes, C.O., Jette, C.A., Abernathy, M.E., Dam, K.A., Esswein, S.R., Gristick, H.B., Malyutin,  
549 A.G., Sharaf, N.G., Huey-Tubman, K.E., Lee, Y.E., *et al.* (2020a). SARS-CoV-2 neutralizing  
550 antibody structures inform therapeutic strategies. *Nature* 588, 682-687.  
551 Barnes, C.O., West, A.P., Jr., Huey-Tubman, K.E., Hoffmann, M.A.G., Sharaf, N.G., Hoffman,  
552 P.R., Koranda, N., Gristick, H.B., Gaebler, C., Muecksch, F., *et al.* (2020b). Structures of Human  
553 Antibodies Bound to SARS-CoV-2 Spike Reveal Common Epitopes and Recurrent Features of  
554 Antibodies. *Cell* 182, 828-842.e816.  
555 Beigel, J.H., Tomashek, K.M., Dodd, L.E., Mehta, A.K., Zingman, B.S., Kalil, A.C., Hohmann,  
556 E., Chu, H.Y., Luetkemeyer, A., Kline, S., *et al.* (2020). Remdesivir for the Treatment of Covid-  
557 19 — Final Report. *New England Journal of Medicine* 383, 1813-1826.  
558 Brown, A.J., Won, J.J., Graham, R.L., Dinno, K.H., 3rd, Sims, A.C., Feng, J.Y., Cihlar, T.,  
559 Denison, M.R., Baric, R.S., and Sheahan, T.P. (2019). Broad spectrum antiviral remdesivir  
560 inhibits human endemic and zoonotic deltacoronaviruses with a highly divergent RNA  
561 dependent RNA polymerase. *Antiviral Res* 169, 104541.  
562 Chen, R.E., Zhang, X., Case, J.B., Winkler, E.S., Liu, Y., VanBlargan, L.A., Liu, J., Errico, J.M.,  
563 Xie, X., Suryadevara, N., *et al.* (2021). Resistance of SARS-CoV-2 variants to neutralization by  
564 monoclonal and serum-derived polyclonal antibodies. *Nat Med*.  
565 de Wit, E., Feldmann, F., Cronin, J., Jordan, R., Okumura, A., Thomas, T., Scott, D., Cihlar, T.,  
566 and Feldmann, H. (2020). Prophylactic and therapeutic remdesivir (GS-5734) treatment in the  
567 rhesus macaque model of MERS-CoV infection. *Proc Natl Acad Sci U S A* 117, 6771-6776.  
568 Dieterle, M.E., Haslwanter, D., Bortz, R.H., Wirchnianski, A.S., Lasso, G., Vergnolle, O.,  
569 Abbasi, S.A., Fels, J.M., Laudermilch, E., Florez, C., *et al.* (2020). A replication-competent  
570 vesicular stomatitis virus for studies of SARS-CoV-2 spike-mediated cell entry and its inhibition.  
571 *bioRxiv*, 2020.2005.2020.105247.  
572 Dinno, K.H., 3rd, Leist, S.R., Schafer, A., Edwards, C.E., Martinez, D.R., Montgomery, S.A.,  
573 West, A., Yount, B.L., Jr., Hou, Y.J., Adams, L.E., *et al.* (2020). A mouse-adapted model of  
574 SARS-CoV-2 to test COVID-19 countermeasures. *Nature* 586, 560-566.  
575 Gaebler, C., Wang, Z., Lorenzi, J.C.C., Muecksch, F., Finkin, S., Tokuyama, M., Cho, A.,  
576 Jankovic, M., Schaefer-Babajew, D., Oliveira, T.Y., *et al.* (2021). Evolution of antibody  
577 immunity to SARS-CoV-2. *Nature*.  
578 Gottlieb, R.L., Nirula, A., Chen, P., Boscia, J., Heller, B., Morris, J., Huhn, G., Cardona, J.,  
579 Mocherla, B., Stosor, V., *et al.* (2021). Effect of Bamlanivimab as Monotherapy or in  
580 Combination With Etesevimab on Viral Load in Patients With Mild to Moderate COVID-19: A  
581 Randomized Clinical Trial. *Jama*.  
582 Hansen, J., Baum, A., Pascal, K.E., Russo, V., Giordano, S., Wloga, E., Fulton, B.O., Yan, Y.,  
583 Koon, K., Patel, K., *et al.* (2020). Studies in humanized mice and convalescent humans yield a  
584 SARS-CoV-2 antibody cocktail. *Science* 369, 1010-1014.



585 Jones, B.E., Brown-Augsburger, P.L., Corbett, K.S., Westendorf, K., Davies, J., Cujec, T.P.,  
586 Wiethoff, C.M., Blackbourne, J.L., Heinz, B.A., Foster, D., *et al.* (2020). LY-CoV555, a rapidly  
587 isolated potent neutralizing antibody, provides protection in a non-human primate model of  
588 SARS-CoV-2 infection. *bioRxiv*.

589 Kalil, A.C., Patterson, T.F., Mehta, A.K., Tomashek, K.M., Wolfe, C.R., Ghazaryan, V.,  
590 Marconi, V.C., Ruiz-Palacios, G.M., Hsieh, L., Kline, S., *et al.* (2020). Baricitinib plus  
591 Remdesivir for Hospitalized Adults with Covid-19. *New England Journal of Medicine*.

592 Leist, S.R., Dinnon, K.H., 3rd, Schäfer, A., Tse, L.V., Okuda, K., Hou, Y.J., West, A., Edwards,  
593 C.E., Sanders, W., Fritch, E.J., *et al.* (2020). A Mouse-Adapted SARS-CoV-2 Induces Acute  
594 Lung Injury and Mortality in Standard Laboratory Mice. *Cell* *183*, 1070-1085.e1012.

595 Li, D., Edwards, R.J., Manne, K., Martinez, D.R., Schäfer, A., Alam, S.M., Wiehe, K., Lu, X.,  
596 Parks, R., Sutherland, L.L., *et al.* (2021). The functions of SARS-CoV-2 neutralizing and  
597 infection-enhancing antibodies in vitro and in mice and nonhuman primates. *bioRxiv*.

598 Liu, Y., Yan, L.M., Wan, L., Xiang, T.X., Le, A., Liu, J.M., Peiris, M., Poon, L.L.M., and  
599 Zhang, W. (2020). Viral dynamics in mild and severe cases of COVID-19. *Lancet Infect Dis* *20*,  
600 656-657.

601 Martin, R., Li, J., Parvangada, A., Perry, J., Cihlar, T., Mo, H., Porter, D., and Svarovskaia, E.  
602 (2021). Genetic conservation of SARS-CoV-2 RNA replication complex in globally circulating  
603 isolates and recently emerged variants from humans and minks suggests minimal pre-existing  
604 resistance to remdesivir. *Antiviral Res* *188*, 105033.

605 Matute-Bello, G., Downey, G., Moore, B.B., Groshong, S.D., Matthay, M.A., Slutsky, A.S., and  
606 Kuebler, W.M. (2011). An official American Thoracic Society workshop report: features and  
607 measurements of experimental acute lung injury in animals. *Am J Respir Cell Mol Biol* *44*, 725-  
608 738.

609 Menachery, V.D., Gralinski, L.E., Baric, R.S., and Ferris, M.T. (2015). New Metrics for  
610 Evaluating Viral Respiratory Pathogenesis. *PLoS One* *10*, e0131451.

611 Montagutelli, X., Prot, M., Levillayer, L., Salazar, E.B., Jouvion, G., Conquet, L., Donati, F.,  
612 Albert, M., Gambaro, F., Behillil, S., *et al.* (2021). The B.1.351 and P.1 variants extend SARS-  
613 CoV-2 host range to mice. *bioRxiv*, 2021.2003.2018.436013.

614 Planas, D., Bruel, T., Grzelak, L., Guivel-Benhassine, F., Staropoli, I., Porrot, F., Planchais, C.,  
615 Buchrieser, J., Rajah, M.M., Bishop, E., *et al.* (2021). Sensitivity of infectious SARS-CoV-2  
616 B.1.1.7 and B.1.351 variants to neutralizing antibodies. *Nature Medicine*.

617 Pruijssers, A.J., George, A.S., Schafer, A., Leist, S.R., Gralinski, L.E., Dinnon, K.H., 3rd, Yount,  
618 B.L., Agostini, M.L., Stevens, L.J., Chappell, J.D., *et al.* (2020). Remdesivir Inhibits SARS-  
619 CoV-2 in Human Lung Cells and Chimeric SARS-CoV Expressing the SARS-CoV-2 RNA  
620 Polymerase in Mice. *Cell Rep* *32*, 107940.

621 Robbiani, D.F., Gaebler, C., Muecksch, F., Lorenzi, J.C.C., Wang, Z., Cho, A., Agudelo, M.,  
622 Barnes, C.O., Gazumyan, A., Finkin, S., *et al.* (2020). Convergent antibody responses to SARS-  
623 CoV-2 in convalescent individuals. *Nature* *584*, 437-442.

624 Rogers, T.F., Zhao, F., Huang, D., Beutler, N., Burns, A., He, W.T., Limbo, O., Smith, C., Song,  
625 G., Woehl, J., *et al.* (2020). Isolation of potent SARS-CoV-2 neutralizing antibodies and  
626 protection from disease in a small animal model. *Science* *369*, 956-963.

627 Schäfer, A., Muecksch, F., Lorenzi, J.C.C., Leist, S.R., Cipolla, M., Bournazos, S., Schmidt, F.,  
628 Maison, R.M., Gazumyan, A., Martinez, D.R., *et al.* (2021). Antibody potency, effector function,  
629 and combinations in protection and therapy for SARS-CoV-2 infection in vivo. *J Exp Med* *218*.

630 Schmidt, M.E., Knudson, C.J., Hartwig, S.M., Pewe, L.L., Meyerholz, D.K., Langlois, R.A.,  
631 Harty, J.T., and Varga, S.M. (2018). Memory CD8 T cells mediate severe immunopathology  
632 following respiratory syncytial virus infection. *PLoS Pathog* 14, e1006810.  
633 Sheahan, T.P., Sims, A.C., Graham, R.L., Menachery, V.D., Gralinski, L.E., Case, J.B., Leist,  
634 S.R., Pyrc, K., Feng, J.Y., Trantcheva, I., *et al.* (2017). Broad-spectrum antiviral GS-5734  
635 inhibits both epidemic and zoonotic coronaviruses. *Sci Transl Med* 9.  
636 Sheahan, T.P., Sims, A.C., Leist, S.R., Schäfer, A., Won, J., Brown, A.J., Montgomery, S.A.,  
637 Hogg, A., Babusis, D., Clarke, M.O., *et al.* (2020). Comparative therapeutic efficacy of  
638 remdesivir and combination lopinavir, ritonavir, and interferon beta against MERS-CoV. *Nature*  
639 *Communications* 11, 222.  
640 Wang, D., Hu, B., Hu, C., Zhu, F., Liu, X., Zhang, J., Wang, B., Xiang, H., Cheng, Z., Xiong,  
641 Y., *et al.* (2020). Clinical Characteristics of 138 Hospitalized Patients With 2019 Novel  
642 Coronavirus-Infected Pneumonia in Wuhan, China. *Jama* 323, 1061-1069.  
643 Wang, L., Zhou, T., Zhang, Y., Yang, E.S., Schramm, C.A., Shi, W., Pegu, A., Oloninyi, O.K.,  
644 Ransier, A., Darko, S., *et al.* (2021a). Antibodies with potent and broad neutralizing activity  
645 against antigenically diverse and highly transmissible SARS-CoV-2 variants. *bioRxiv*.  
646 Wang, P., Nair, M.S., Liu, L., Iketani, S., Luo, Y., Guo, Y., Wang, M., Yu, J., Zhang, B.,  
647 Kwong, P.D., *et al.* (2021b). Antibody resistance of SARS-CoV-2 variants B.1.351 and B.1.1.7.  
648 *Nature*.  
649 Wang, Z., Schmidt, F., Weisblum, Y., Muecksch, F., Barnes, C.O., Finkin, S., Schaefer-  
650 Babajew, D., Cipolla, M., Gaebler, C., Lieberman, J.A., *et al.* (2021c). mRNA vaccine-elicited  
651 antibodies to SARS-CoV-2 and circulating variants. *Nature*.  
652 Weinreich, D.M., Sivapalasingam, S., Norton, T., Ali, S., Gao, H., Bhore, R., Musser, B.J., Soo,  
653 Y., Rofail, D., Im, J., *et al.* (2020). REGN-COV2, a Neutralizing Antibody Cocktail, in  
654 Outpatients with Covid-19. *New England Journal of Medicine*.  
655 Williamson, B.N., Feldmann, F., Schwarz, B., Meade-White, K., Porter, D.P., Schulz, J., van  
656 Doremalen, N., Leighton, I., Yinda, C.K., Perez-Perez, L., *et al.* (2020). Clinical benefit of  
657 remdesivir in rhesus macaques infected with SARS-CoV-2. *Nature* 585, 273-276.  
658 Yang, X., Yu, Y., Xu, J., Shu, H., Xia, J., Liu, H., Wu, Y., Zhang, L., Yu, Z., Fang, M., *et al.*  
659 (2020). Clinical course and outcomes of critically ill patients with SARS-CoV-2 pneumonia in  
660 Wuhan, China: a single-centered, retrospective, observational study. *Lancet Respir Med* 8, 475-  
661 481.  
662 Zheng, S., Fan, J., Yu, F., Feng, B., Lou, B., Zou, Q., Xie, G., Lin, S., Wang, R., Yang, X., *et al.*  
663 (2020). Viral load dynamics and disease severity in patients infected with SARS-CoV-2 in  
664 Zhejiang province, China, January-March 2020: retrospective cohort study. *Bmj* 369, m1443.  
665 Zhou, F., Yu, T., Du, R., Fan, G., Liu, Y., Liu, Z., Xiang, J., Wang, Y., Song, B., Gu, X., *et al.*  
666 (2020a). Clinical course and risk factors for mortality of adult inpatients with COVID-19 in  
667 Wuhan, China: a retrospective cohort study. *Lancet* 395, 1054-1062.  
668 Zhou, P., Yang, X.L., Wang, X.G., Hu, B., Zhang, L., Zhang, W., Si, H.R., Zhu, Y., Li, B.,  
669 Huang, C.L., *et al.* (2020b). A pneumonia outbreak associated with a new coronavirus of  
670 probable bat origin. *Nature* 579, 270-273.  
671 Zhu, N., Zhang, D., Wang, W., Li, X., Yang, B., Song, J., Zhao, X., Huang, B., Shi, W., Lu, R.,  
672 *et al.* (2020). A Novel Coronavirus from Patients with Pneumonia in China, 2019. *New England*  
673 *Journal of Medicine* 382, 727-733.

674 Zost, S.J., Gilchuk, P., Case, J.B., Binshtein, E., Chen, R.E., Nkolola, J.P., Schäfer, A., Reidy,  
675 J.X., Trivette, A., Nargi, R.S., *et al.* (2020a). Potently neutralizing and protective human  
676 antibodies against SARS-CoV-2. *Nature* 584, 443-449.  
677 Zost, S.J., Gilchuk, P., Chen, R.E., Case, J.B., Reidy, J.X., Trivette, A., Nargi, R.S., Sutton, R.E.,  
678 Suryadevara, N., Chen, E.C., *et al.* (2020b). Rapid isolation and profiling of a diverse panel of  
679 human monoclonal antibodies targeting the SARS-CoV-2 spike protein. *Nat Med* 26, 1422-1427.  
680

681

682

683

684

685

686

687

688

689

690

691

692

693

694

695

696

697

698

699

700 **Figure legends**

701

702 **Figure 1. The prophylactic and therapeutic efficacy of RDV against SARS-CoV-2 in mice.**

703 (A) % starting weight in prophylactically treated mice with RDV at 12 hours before infection,

704 and therapeutically at 12, 24, and 48 hours post infection. From left to right, light blue bars

705 denote -12 hours prophylactic treatment, orange bars denote +12 hours therapeutic treatment,

706 purple bars denote +24 hours therapeutic treatment, aqua bars denote +48 hours therapeutic

707 treatment, and grey bars denote vehicle treated mice.

708 (B) Lung viral titers in prophylactically and therapeutically treated mice with RDV. Limit of

709 detection (LoD).

710 (C) Lung discoloration score in prophylactically and therapeutically treated mice with RDV.

711 (D-E) Lung pathology in prophylactically and therapeutically treated mice with RDV.

712 (F) Pulmonary function in prophylactically and therapeutically treated mice with RDV. P values

713 are from a 2-way ANOVA after Sidak's multiple comparisons test.

714

715 **Figure 2. The prophylactic and therapeutic efficacy of mAbs against SARS-CoV-2 in mice.**

716 (A) % starting weight in prophylactically treated mice with C144 + C135 at 12 hours before

717 infection, and therapeutically at 12, 24, and 48 hours post infection. From left to right, light blue

718 bars denote -12 hours prophylactic treatment, orange bars denote +12 hours therapeutic

719 treatment, purple bars denote +24 hours therapeutic treatment, aqua bars denote +48 hours

720 therapeutic treatment, and grey bars denote vehicle treated mice.

721 (B) Lung viral titers in prophylactically and therapeutically treated mice with C144 + C135.

722 (C) Lung discoloration score in prophylactically and therapeutically treated mice with C144 +  
723 C135.

724 (D-E) Lung pathology in prophylactically and therapeutically treated mice with C144 + C135.

725 (F) Pulmonary function in prophylactically and therapeutically treated mice with C144 + C135. P  
726 values are from a 2-way ANOVA after Sidak's multiple comparisons test.

727

728 **Figure 3. The therapeutic efficacy of RDV and mAbs as single agents and in combination at**  
729 **36 hours post infection in SARS-CoV-2-infected mice.**

730 (A) % starting weight in therapeutically treated mice with vehicle + HIV mAb, vehicle + C144 +  
731 C135, RDV + HIV mAb, and RDV + C144 + C135 at 36 hours post infection. From left to right,  
732 grey bars denote vehicle/control mAb treated mice, yellow bars denote vehicle/mAb therapeutic  
733 treatment, blue bars denote RDV/control mAb therapeutic treatment, and orange bars denote  
734 RDV/mAb therapeutic treatment.

735 (B) Day 3 post infection lung viral titers in therapeutically treated mice with single agents and  
736 combination therapy. "Veh." signifies vehicle treatment.

737 (C) Day 5 post infection lung viral titers in therapeutically treated mice with single agents and  
738 combination therapy.

739 (D) Lung discoloration scores in therapeutically treated mice with single agents and combination  
740 therapy.

741 (E) Pulmonary function in therapeutically treated mice with vehicle + HIV mAb and RDV +  
742 C144 + C135. P values are from a 2-way ANOVA after Sidak's multiple comparisons test.

743

744 **Figure 4. The prophylactic and therapeutic efficacy of C144 + C135 against SARS-CoV-2**

745 **B.1.351 in aged mice.**

746 (A) % starting weight in prophylactically treated mice with C144 + C135 at 12 hours before  
747 infection, and therapeutically at 12 post infection. From left to right, light blue bars denote -12  
748 hours prophylactic treatment, orange bars denote +12 hours therapeutic treatment, and grey bars  
749 denote prophylactically treated mice with HIV mAb.

750 (B-C) Lung viral titers at day 3 and 5 post infection in prophylactically and therapeutically  
751 treated mice with C144 + C135 and HIV mAb negative controls.

752 (D-E) Sugenomic Envelope (E) RNA copies/lobe in prophylactically and therapeutically treated  
753 mice with C144 + C135 and HIV mAb.

754 (F-G) Sugenomic Envelope (N) RNA copies/lobe in prophylactically and therapeutically treated  
755 mice with C144 + C135 and HIV mAb.

756 (H-I) Lung discoloration at day 3 and 5 post infection in prophylactically and therapeutically  
757 treated mice with C144 + C135 and HIV mAb. P values are from a 1-way ANOVA following  
758 Dunnett's multiple comparisons.

759

760

761

762

763

764

765

766

767 **Supplemental figure legends**

768

769 **Figure S1. Lung pathology of SARS-CoV-2-infected mice treated with RDV and vehicle**  
770 **prophylactically and therapeutically.**

771 Pathologic features of acute lung injury were scored using two separate tools: the American  
772 Thoracic Society Lung Injury Scoring (ATS ALI) system. Using this ATS ALI system, we  
773 created an aggregate score for the following features: neutrophils in the alveolar and interstitial  
774 space, hyaline membranes, proteinaceous debris filling the air spaces, and alveolar septal  
775 thickening. Three randomly chosen high power ( $\times 60$ ) fields of diseased lung were assessed per  
776 mouse. Representative images are shown from vehicle and RDV-treated mice. Symbols  
777 identifying example features of disease are indicated in the figure. All images were taken at the  
778 same magnification. The black bar indicates 100  $\mu\text{m}$  scale.

779

780 **Figure S2. Lung pathology of SARS-CoV-2-infected mice treated with C144 + C135 and an**  
781 **HIV mAb prophylactically and therapeutically.**

782 Pathologic features of acute lung injury were scored using two separate tools: the American  
783 Thoracic Society Lung Injury Scoring (ATS ALI) system. Using this ATS ALI system, we  
784 created an aggregate score for the following features: neutrophils in the alveolar and interstitial  
785 space, hyaline membranes, proteinaceous debris filling the air spaces, and alveolar septal  
786 thickening. Three randomly chosen high power ( $\times 60$ ) fields of diseased lung were assessed per  
787 mouse. Representative images are shown from HIV mAb and C144 + C135-treated mice.  
788 Symbols identifying example features of disease are indicated in the figure. All images were  
789 taken at the same magnification. The black bar indicates 100  $\mu\text{m}$  scale.

790

791 **Figure S3. The prophylactic efficacy of mAb monotherapy against SARS-CoV-2 in mice**  
792 **treated at 12 hours before infection.**

793 (A) % starting weight in therapeutically treated mice with C144, C135, or an HIV mAb at 12  
794 hours before infection.

795 (B) Lung viral titers in therapeutically treated mice at 12 hours before infection.

796 (C) Lung discoloration score in therapeutically treated mice at 12 hours before infection.

797 (D-E) Lung pathology in therapeutically treated mice at 12 hours before infection. P values are  
798 from a 2-way ANOVA after Sidak's multiple comparisons test.

799

800 **Figure S4. The therapeutic efficacy of mAb monotherapy against SARS-CoV-2 in mice**  
801 **treated at 12 hours post infection.**

802 (A) % starting weight in therapeutically treated mice with C144, C135, or an HIV mAb at 12  
803 hours post infection.

804 (B) Lung viral titers in therapeutically treated mice at 12 hours post infection.

805 (C) Lung discoloration score in therapeutically treated mice at 12 hours post infection.

806 (D-E) Lung pathology in therapeutically treated mice at 12 hours post infection. P values are  
807 from a 2-way ANOVA after Sidak's multiple comparisons test.

808

809 **Figure S5. The therapeutic efficacy of mAb monotherapy against SARS-CoV-2 in mice**  
810 **treated at 24 hours post infection.**

811 (A) % starting weight in therapeutically treated mice with C144, C135, or an HIV mAb at 24  
812 hours post infection.



813 (B) Lung viral titers in therapeutically treated mice at 24 hours post infection.

814 (C) Lung discoloration score in therapeutically treated mice at 24 hours post infection.

815 (D-E) Lung pathology in therapeutically treated mice at 24 hours post infection. P values are

816 from a 2-way ANOVA after Sidak's multiple comparisons test.

817

818 **Figure S6. The therapeutic efficacy of mAb monotherapy against SARS-CoV-2 in mice**

819 **treated at 48 hours post infection.**

820 (A) % starting weight in therapeutically treated mice with C144, C135, or an HIV mAb at 48

821 hours post infection.

822 (B) Lung viral titers in therapeutically treated mice at 48 hours post infection.

823 (C) Lung discoloration score in therapeutically treated mice at 48 hours post infection.

824 (D-E) Lung pathology in therapeutically treated mice at 48 hours post infection. P values are

825 from a 2-way ANOVA after Sidak's multiple comparisons test.

826

827 **Figure S7. The therapeutic efficacy of RDV and mAbs as single agents and in combination**

828 **at 24 hours post infection in SARS-CoV-2-infected mice.**

829 (A) % starting weight in therapeutically treated mice with vehicle + HIV mAb, vehicle + C144 +

830 C135, RDV + HIV mAb, and RDV + C144 + C135 at 24 hours post infection through day 12.

831 From left to right, grey bars denote vehicle/control mAb treated mice, yellow bars denote

832 vehicle/mAb therapeutic treatment, blue bars denote RDV/control mAb therapeutic treatment,

833 and orange bars denote RDV/mAb therapeutic treatment.

834 (B) % mortality in therapeutically treated mice with single agents and combination therapy.

835 (C) Lung discoloration score in therapeutically treated mice with single agents and combination

836 therapy. “Veh.” signifies vehicle treatment.

837 (D) Pulmonary function in therapeutically treated mice with vehicle + HIV mAb and RDV +

838 C144 + C135. P values are from a 2-way ANOVA after Sidak’s multiple comparisons test.

839

Figure 1

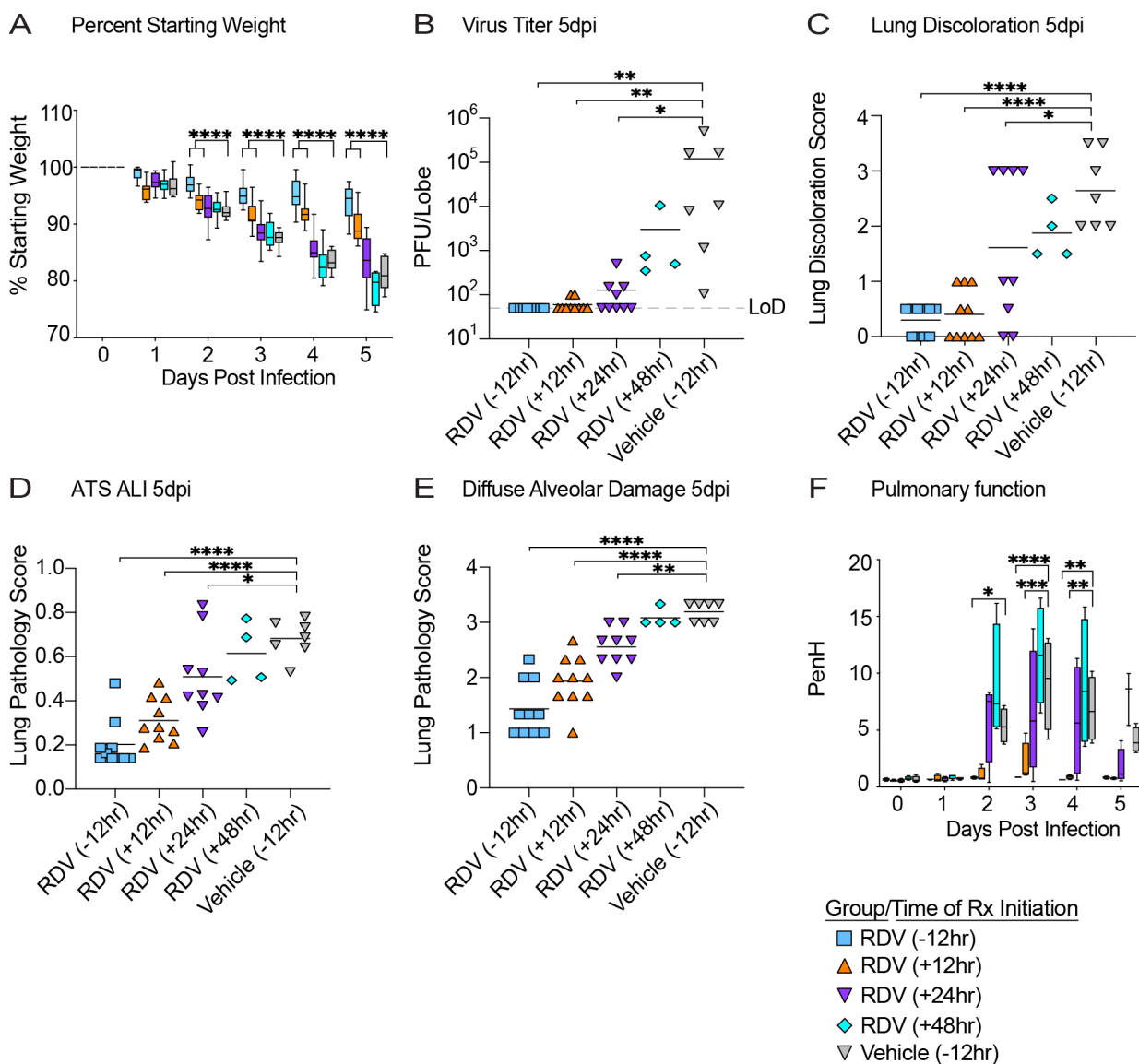


Figure 2

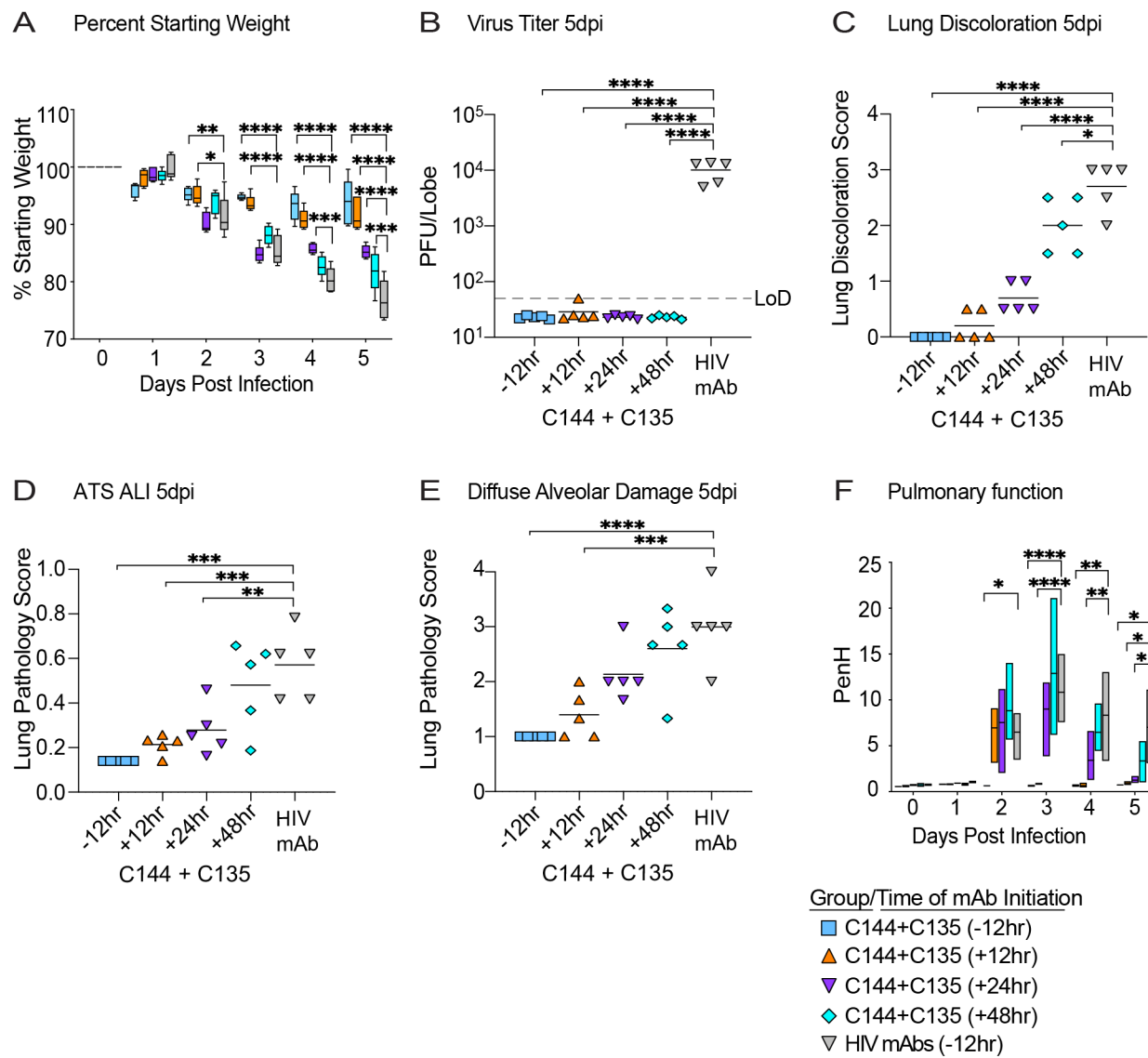


Figure 3

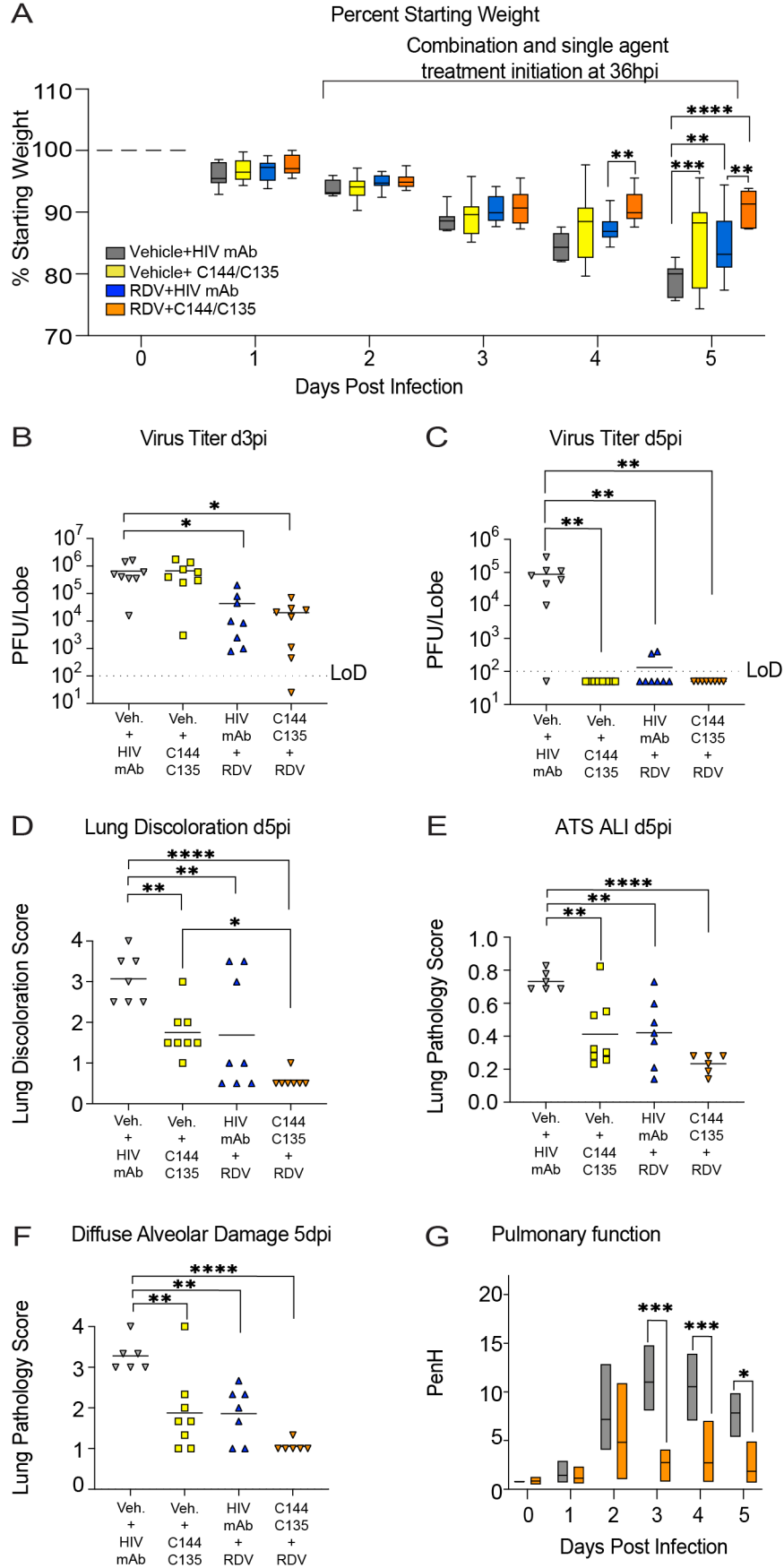


Figure 4

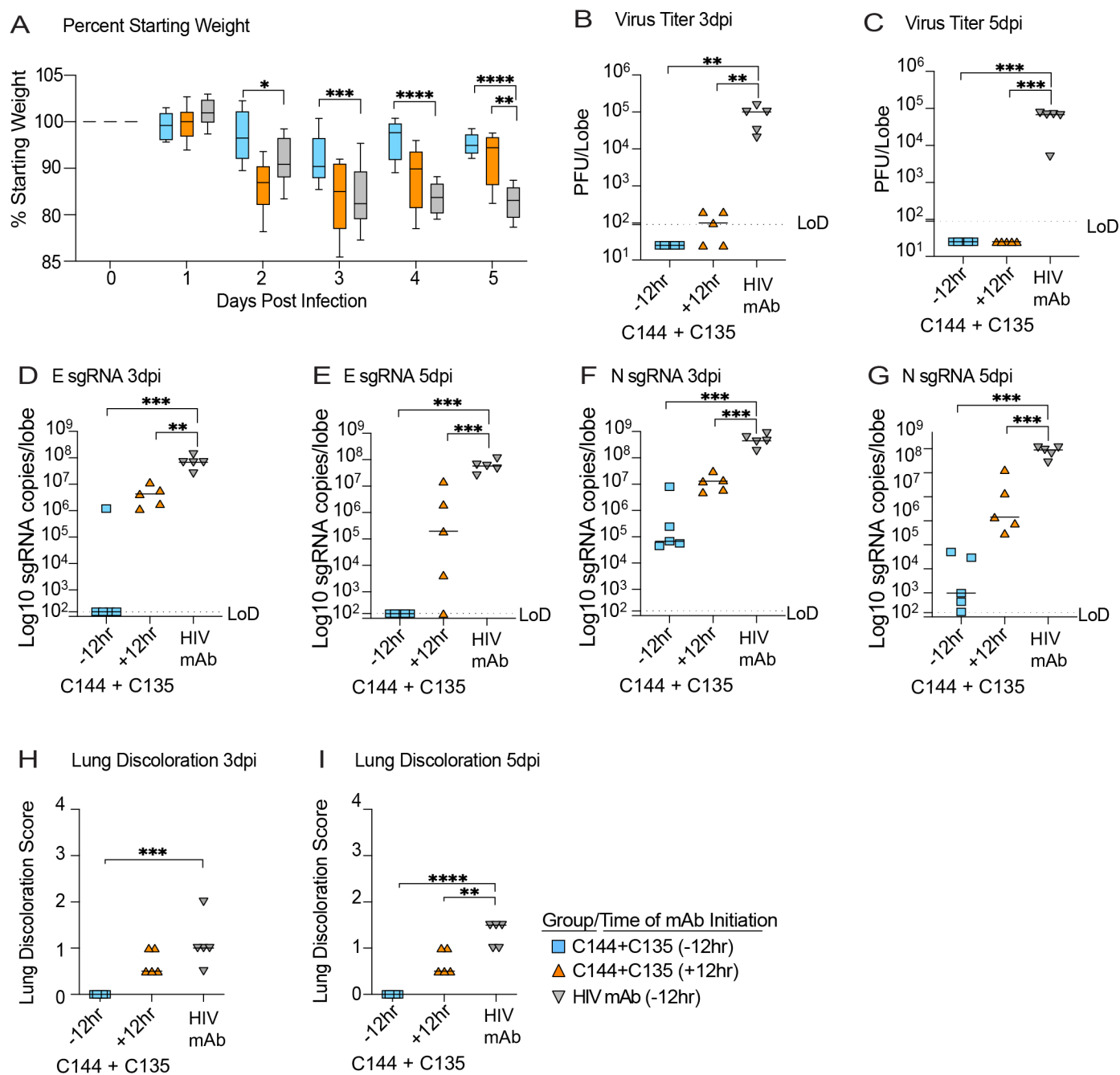
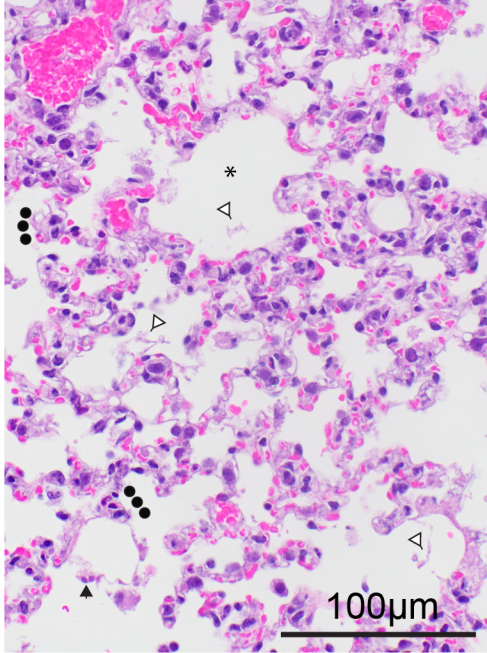
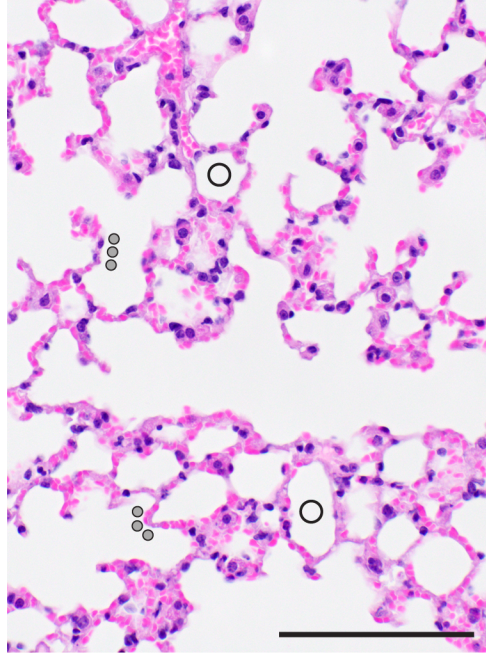


Figure S1

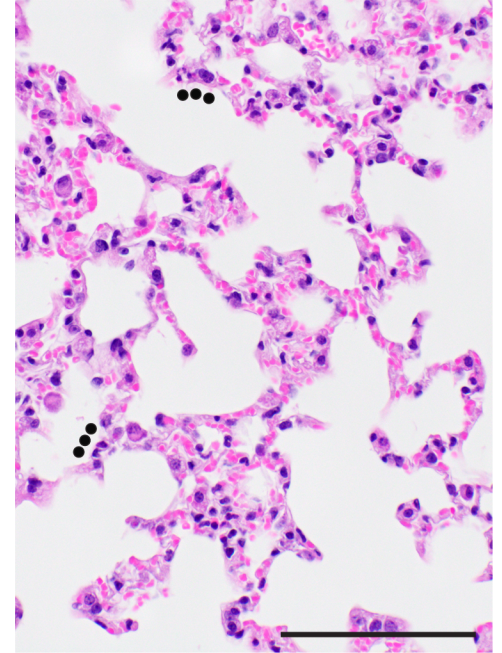
Vehicle



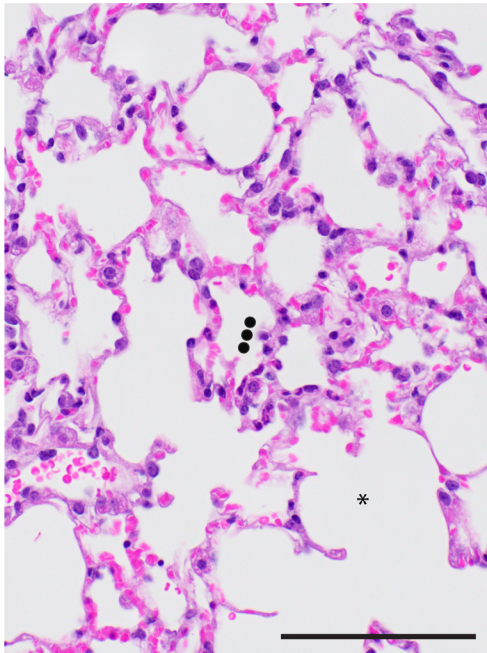
RDV -12hr



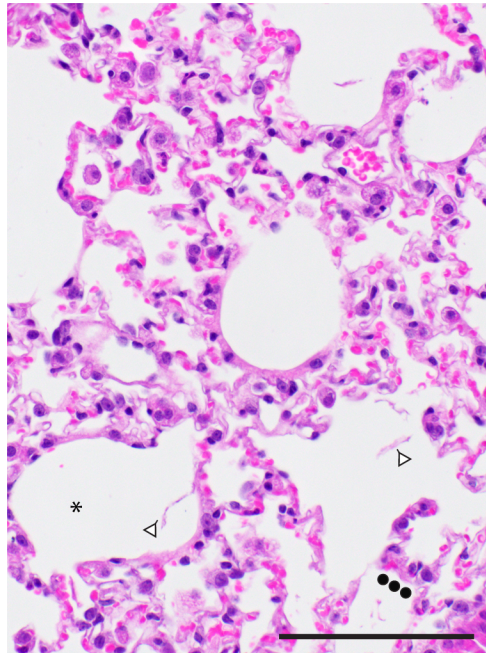
RDV +12hr



RDV +24hr



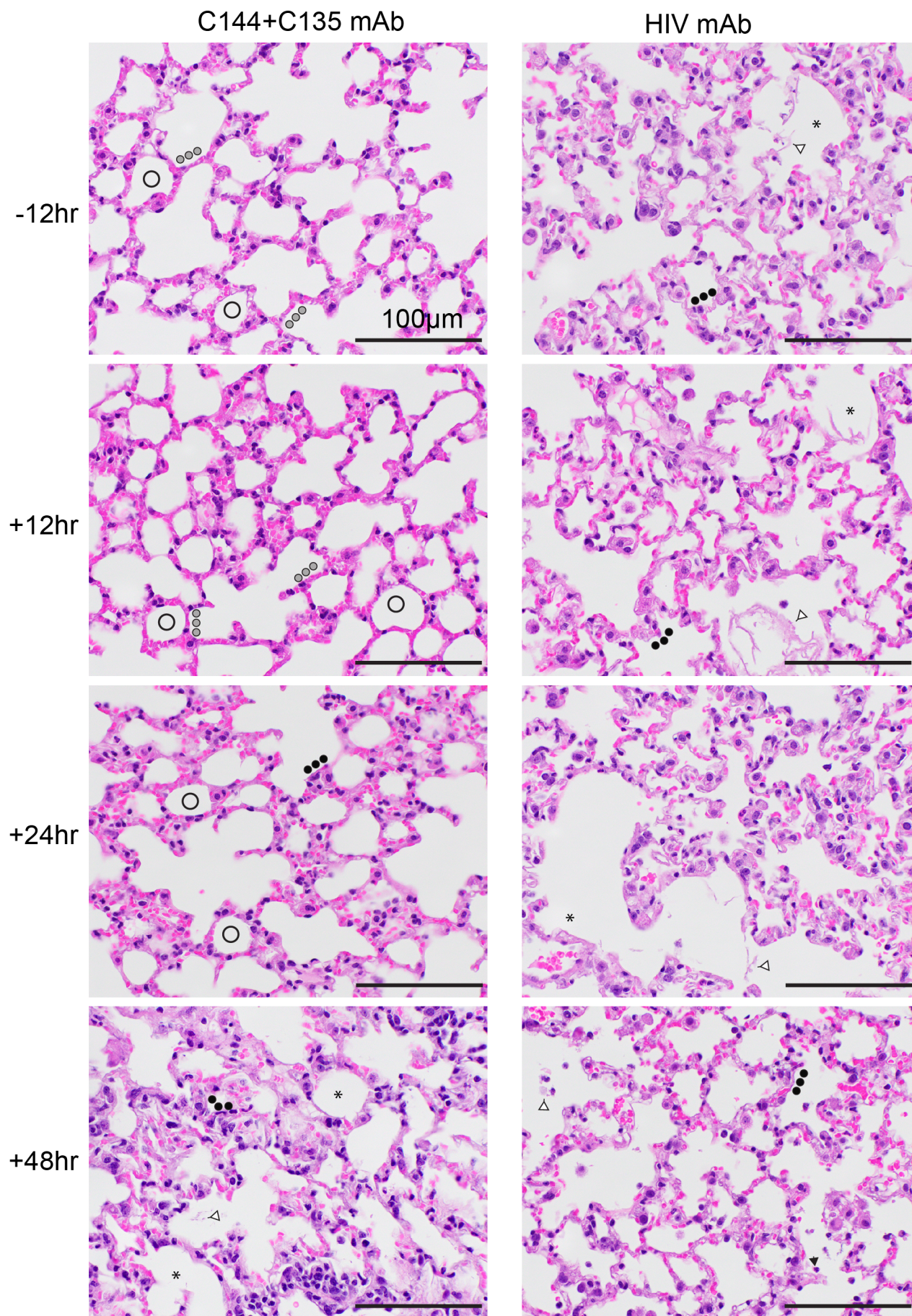
RDV +48hr



**Symbol Key:**

- Normal septal wall thickness and cellularity
- Normal clear airspace of alveolar sac
- Hypercellular alveolar septae
- \* Loss of alveolar septal architecture
- ▲ Neutrophil in alveolar space
- ◁ Proteinaceous debris

Figure S2



**Symbol Key:**

○	Normal septal wall thickness and cellularity	●●●	Hypercellular alveolar septae	▲	Neutrophil in alveolar space
○	Normal clear airspace of alveolar sac	*	Loss of alveolar septal architecture	◁	Proteinaceous debris



Figure S3

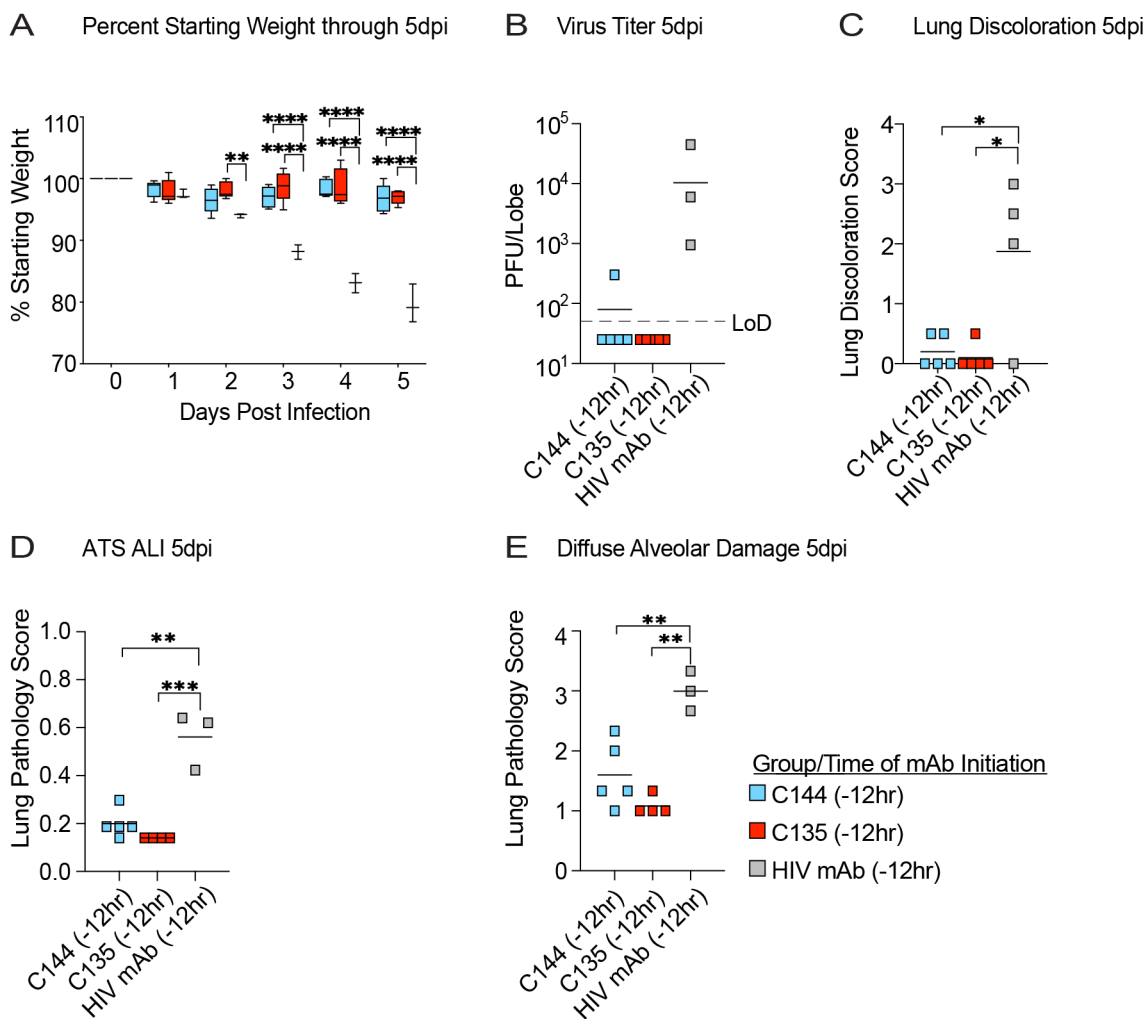


Figure S4

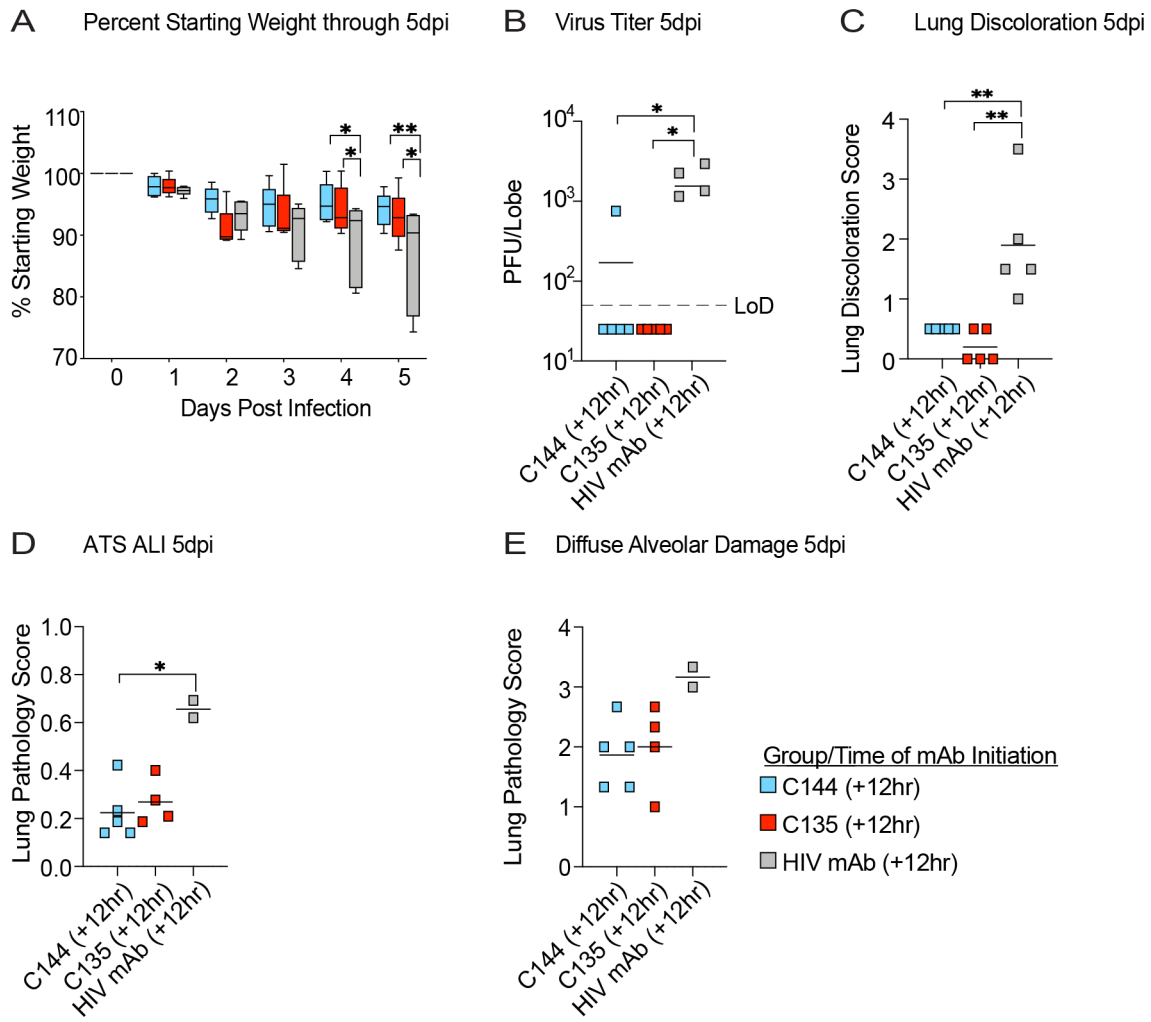


Figure S5

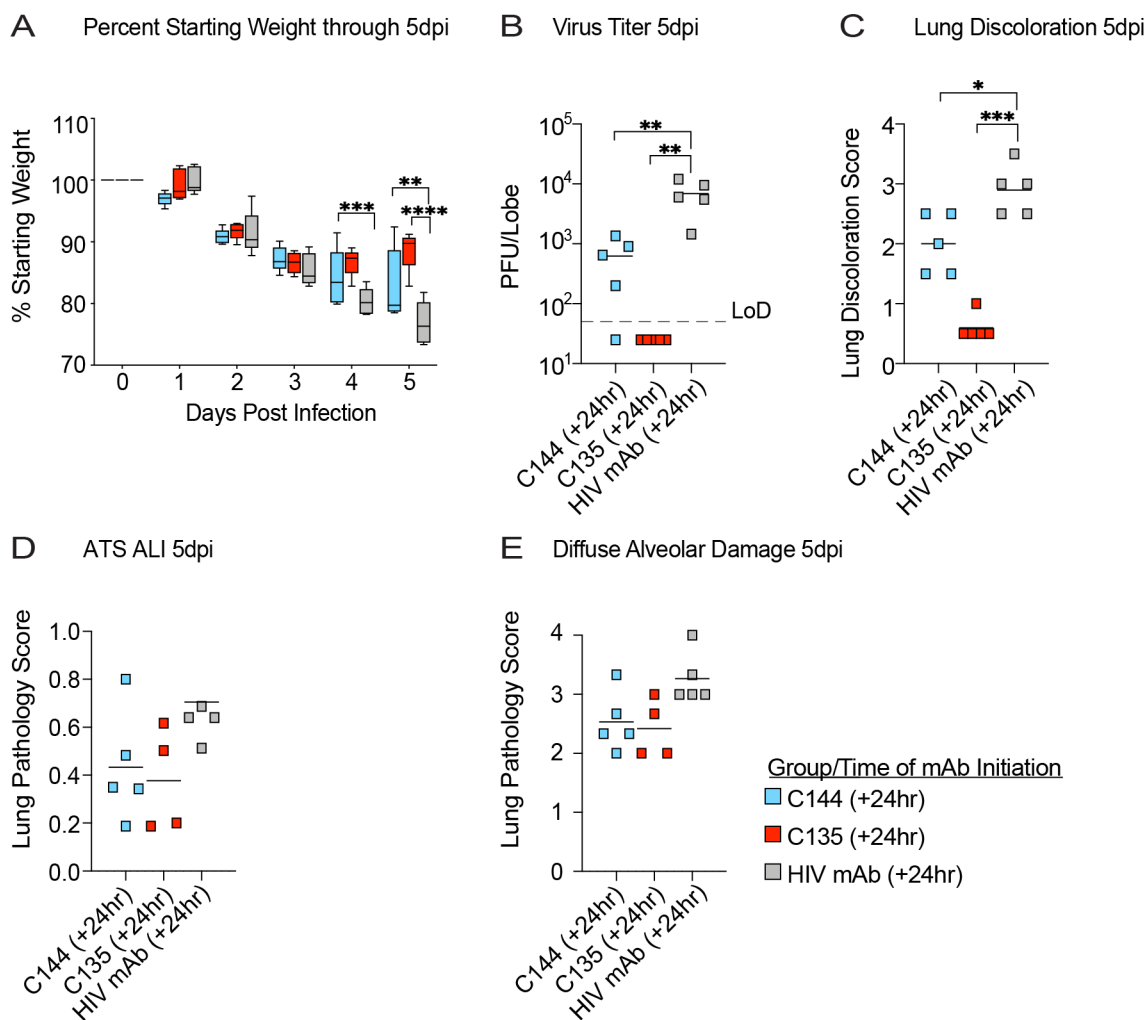


Figure S6

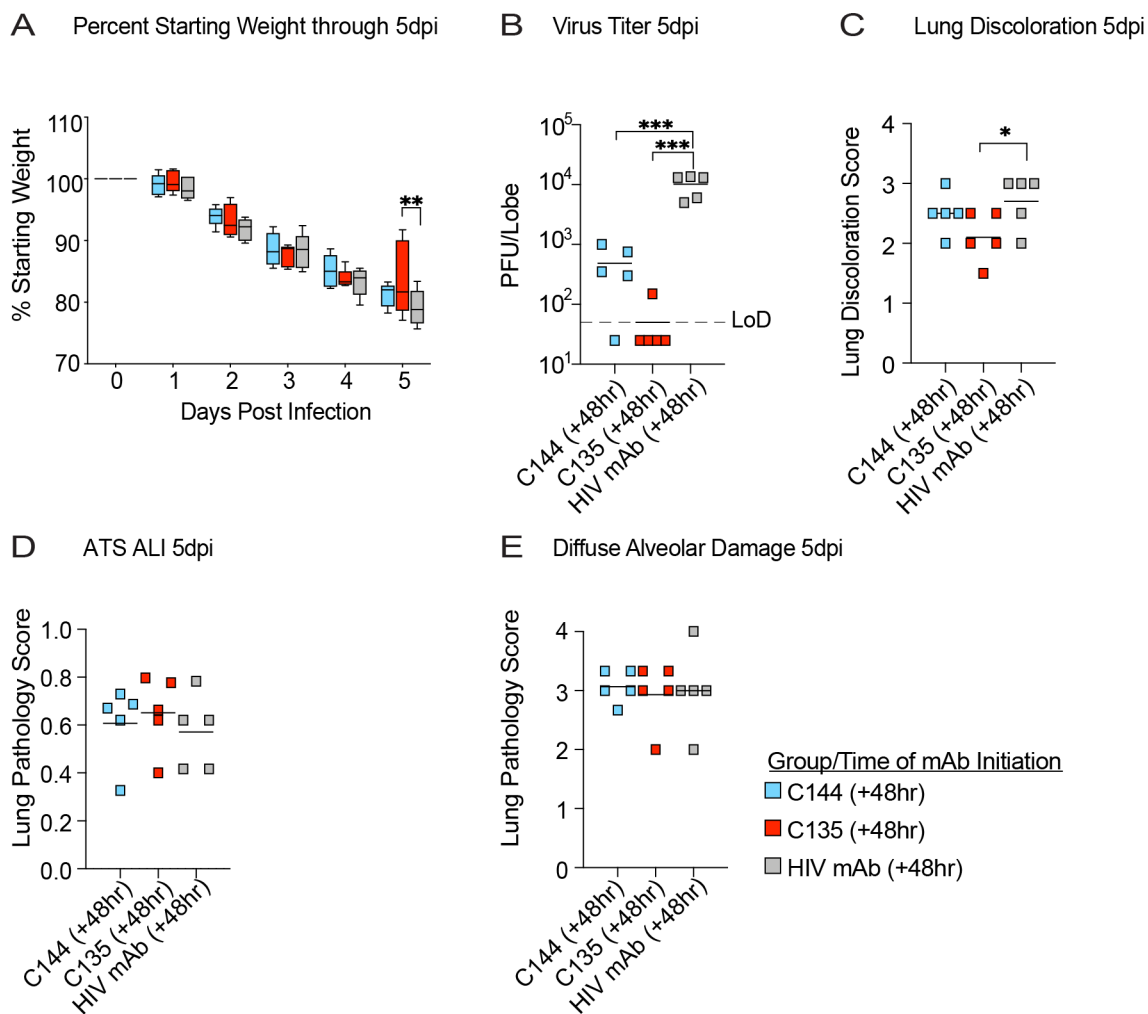


Figure S7

